Journal of Controlled Release 368 (2024) 251–264

Contents lists available at ScienceDirect

Journal of Controlled Release

journal homepage: www.elsevier.com/locate/jconrel

A redox-responsive prodrug for tumor-targeted glutamine restriction

Céline Jasmin Prange [a,b], Nadia Yasmina Ben Sayed [a,b], Bing Feng [a,c], Christine Goepfert [d,e], Daniel Ortiz Trujillo [f], Xile Hu [b,*], Li Tang [a,c,*]

[a] Institute of Bioengineering, École Polytechnique Fédérale de Lausanne (EPFL), Lausanne CH-1015, Switzerland
[b] Institute of Chemical Sciences and Engineering, École Polytechnique Fédérale de Lausanne (EPFL), Lausanne CH-1015, Switzerland
[c] Institute of Materials Science & Engineering, École Polytechnique Fédérale de Lausanne (EPFL), Lausanne CH-1015, Switzerland
[d] Histology Core Facility, École Polytechnique Fédérale de Lausanne (EPFL), Lausanne CH-1015, Switzerland
[e] COMPATH, Institute of Veterinary Pathology, University of Berne, Berne CH-3012, Switzerland
[f] Mass Spectrometry Platform, Institute of Chemical Sciences and Engineering, École Polytechnique Fédérale de Lausanne (EPFL), Lausanne CH-1015, Switzerland

ARTICLE INFO

Keywords:
Glutamine inhibitor
DON (6-Diazo-5-oxo-L-norleucine)
cancer metabolism
Immune modulation
Drug delivery
Safety
Toxicity

ABSTRACT

Modulating the metabolism of cancer cells, immune cells, or both is a promising strategy to potentiate cancer immunotherapy in the nutrient-competitive tumor microenvironment. Glutamine has emerged as an ideal target as cancer cells highly rely on glutamine for replenishing the tricarboxylic acid cycle in the process of aerobic glycolysis. However, non-specific glutamine restriction may induce adverse effects in unconcerned tissues and therefore glutamine inhibitors have achieved limited success in the clinic so far. Here we report the synthesis and evaluation of a redox-responsive prodrug of 6-Diazo-5-oxo-L-norleucine (redox-DON) for tumor-targeted glutamine inhibition. When applied to treat mice bearing subcutaneous CT26 mouse colon carcinoma, redox-DON exhibited equivalent antitumor efficacy but a greatly improved safety profile, particularly, in spleen and gastrointestinal tract, as compared to the state-of-the-art DON prodrug, JHU083. Furthermore, redox-DON synergized with checkpoint blockade antibodies leading to durable cures in tumor-bearing mice. Our results suggest that redox-DON is a safe and effective therapeutic for tumor-targeted glutamine inhibition showing promise for enhanced metabolic modulatory immunotherapy. The approach of reversible chemical modification may be generalized to other metabolic modulatory drugs that suffer from overt toxicity.

1. Introduction

Cancer cells and anti-cancer immune cells both rely on and compete for nutrients in the tumor microenvironment (TME) for growth [1,2]. Modulating metabolism of cancer cells, immune cells, or both has been explored as promising strategies for cancer treatment [3,4]. Among other amino acids, glutamine is the most abundant amino acid in the blood stream and the consumption in cancer cells is often upregulated [5]. It serves as a nitrogen (N)- and carbon (C)-donor in the synthesis of nucleotides, amino acids and amino-sugars which are essential metabolites for cell survival and proliferation [[6]]. As an amino acid, glutamine is incorporated into proteins and co-factors, with a particularly important role as a component of the redox molecule glutathione, which maintains redox homeostasis within cells [7,8]. Though glutamine is a non-essential amino acid and can, in principle, be synthesized *de novo*, highly proliferative cells, such as cancer cells, often rely on glutamine as an anaplerotic substrate for the tricarboxylic acid (TCA) cycle to comply with their energy demands [9,10]. Therefore, exploiting cancer cell dependency on glutamine supply as a metabolic vulnerability is a promising anti-tumor strategy. In addition, glutamine inhibition typically promotes anti-cancer immune cell expansion and function in tumor [11–13]. Glutamine restriction has been reported to direct anti-tumor $CD8^+$ T cells to a long-lived, highly activated phenotype with upregulated oxidative phosphorylation [12], promotes infiltration of inflammatory tumor-associated macrophages (TAMs) [13], and skew macrophages from an M2 to an M1 phenotype [14].

Most of current glutamine inhibitors, such as the clinically investigated CB-839 [15,16], target the glutaminase 1 (GLS1), the most important glutamine-converting enzyme, typically fail to completely hinder cells from using glutamine through other complementary processes [17]. Another type of glutamine inhibitor is glutamine analogue, such as 6-Diazo-5-oxo-L-norleucine (DON), in which the side chain amine group is replaced by a reactive diazomethane unit. DON covalently binds and inhibits glutamine-converting enzymes in their active

* Corresponding author at: Institute of Bioengineering, École Polytechnique Fédérale de Lausanne (EPFL), Lausanne CH-1015, Switzerland.
E-mail addresses: xile.hu@epfl.ch (X. Hu), li.tang@epfl.ch (L. Tang).

https://doi.org/10.1016/j.jconrel.2024.02.031
Received 13 August 2023; Received in revised form 6 February 2024; Accepted 21 February 2024
Available online 29 February 2024

pocket, which completely abrogates the enzymatic activity of a broad spectrum of glutamine-converting enzymes. DON treatments against tumor cells *in vitro* have demonstrated the efficacy of DON against various tumor cell lines [18]. However, previous clinical studies with DON have shown severe dose-limiting toxicity in tissues of the gastrointestinal (GI) tract [19].

The prodrug strategy is an effective way to mitigate toxicities. A prodrug of DON, JHU083, has been developed by protecting both N-terminal and C-terminal sides with enzymatically cleavable pro-moieties [20]. The increased stability of JHU083 in comparison to DON in monkey and human plasma demonstrated the validity of this prodrug approach. However, proteases are prominent in cells of the digestive system and other sites where toxicity had previously been found [21,22]. Therefore, using a tumor-targeting pro-moiety where the DON release would be based on altered physiological conditions specific to the TME could further increase the safety of glutamine inhibitors.

Here we report the synthesis and evaluation of a novel prodrug of DON for tumor-targeted glutamine inhibition. Different tumor-promoting mechanisms have shown to increase glutathione and other reducing agents in the TME and within tumor cells [23,24]. Therefore, we chose a disulfide-based chemical pro-moiety that responds to the increased reducing condition in the TME as demonstrated previously [25–27]. DON was modified with an N-terminal 2-(pyridin-2-yldisulfaneyl)ethyl carbamate and a C-terminal methyl ester to afford a prodrug, termed redox-DON (Scheme 1). We compared redox-DON and JHU083 in multiple *in vitro* and *in vivo* experiments and found that redox-DON exhibited equivalent efficacy, but increased safety in comparison to JHU083. We further showed that redox-DON synergized with checkpoint blockade antibodies and recruited $CD4^+$, dendritic cells, and M1 macrophages to the TME for enhanced therapeutic efficacy in a mouse colon cancer model. The results provide evidence that redox-DON is a promising glutamine inhibitor drug for cancer therapy that outperforms current drugs of the same kind in the clinic. The chemical modification strategy could potentially be applied to other metabolic modulatory drugs. Our findings also provide insight into how immune cells can be metabolically supported to thrive in the immunosuppressive TME.

2. Materials and methods

2.1. Chemical synthesis

2.1.1. Synthesis of compound 1

(*S*)-4-((((9*H*-fluoren-9-yl)methoxy) carbonyl)amino)-5-methoxy-5-oxopentanoic acid (5 g, 13 mmoles, 1 eq.) was dissolved in dichloromethane (20 ml) and cooled to 0 °C. Thionyl chloride (1.8 ml, 24.8 mmoles, 1.9 eq.) was added, followed by *N*,*N*-dimethylformamide (101 μl, 1.3 mmoles, 0.1 eq.). The mixture was refluxed at 40 °C for 4 h until completion of the reaction as monitored by NMR. The reaction mixture was washed with brine, dried over magnesium sulfate, concentrated and purified by flash chromatography (SiO_2, *n*-hexane:EtOAc 50:50). Compound 1 was obtained as a white crystalline powder (4.0 g, 93% yield).

^{1}H NMR (400 MHz, $CDCl_3$) δ 7.80–7.71 (m, 3H), 7.70 (dq, J = 7.4, 1.0 Hz, 1H), 7.46–7.29 (m, 4H), 4.65 (dd, J = 9.4, 2.5 Hz, 1H), 4.58 (dd, J = 10.5, 7.2 Hz, 1H), 4.46 (dd, J = 10.6, 7.3 Hz, 1H), 4.30 (t, J = 7.2 Hz, 1H), 3.74 (s, 3H), 2.71 (ddd, J = 17.6, 10.7, 9.4 Hz, 1H), 2.57 (ddd, J = 17.6, 9.3, 3.1 Hz, 1H), 2.39 (ddt, J = 13.4, 10.7, 9.3 Hz, 1H), 2.19–2.01 (m, 1H).

2.1.2. Synthesis of compound 2

(Trimethylsilyl)diazomethane (2 M in diethyl ether, 6.57 ml, 13.1 mmoles, 1.2 eq.) was dissolved in tetrahydrofuran (50 ml) and cooled to −78 °C. N-butyllithium (2.5 M, 5.47 ml, 13.7 mmoles, 1.25 eq.) was added dropwise over 10 min. The mixture was stirred at −78 °C for 30 min and then transferred in a syringe to a solution of compound 1 (4 g, 10.9 mmoles, 1 eq.), dissolved in tetrahydrofuran (100 ml), cooled to −78 °C. The mixture was stirred for 30 min and then the reaction was quenched by the addition of saturated ammonium chloride in water (100 ml). The aqueous phase was then extracted twice with ethyl acetate (50 ml). The combined organic layers were washed with brine (50 ml), dried over magnesium sulfate and concentrated. The brown crude product was purified by flash chromatography (SiO_2, *n*-hexane:EtOAc 60:40). The product was obtained as a yellow oil (2.25 g, 50% yield).

^{1}H NMR (400 MHz, $CDCl_3$) δ 7.78 (dd, J = 9.3, 7.3 Hz, 3H), 7.76–7.70 (m, 1H), 7.61 (s, 1H), 7.48–7.30 (m, 4H), 4.67 (dd, J = 9.5,

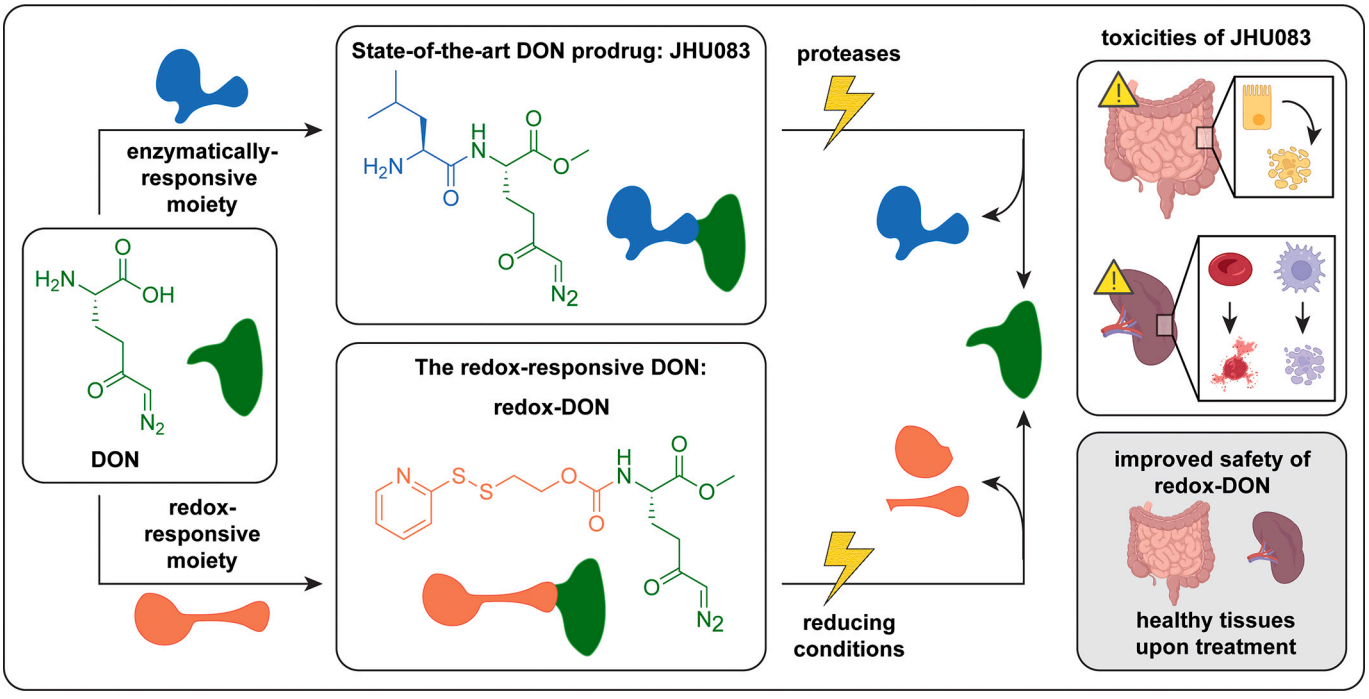

Scheme 1. Schematic illustration of DON and DON-derived prodrugs, JHU083 and redox-DON. We designed a redox-DON that retained the anti-tumor therapeutic effects but minimized adverse effects by specifically targeting the TME.

2.5 Hz, 1H), 4.61 (dd, $J = 10.6$, 7.2 Hz, 1H), 4.48 (dd, $J = 10.6$, 7.3 Hz, 1H), 4.33 (t, $J = 7.2$ Hz, 1H), 3.77 (s, 3H), 2.74 (ddd, $J = 17.5$, 10.7, 9.4 Hz, 1H), 2.59 (ddd, $J = 17.6$, 9.3, 3.1 Hz, 1H), 2.49–2.34 (m, 1H), 2.14 (ddt, $J = 12.7$, 9.4, 2.9 Hz, 1H).

2.1.3. Synthesis of compound 3

Compound 2 (2.25 g, 5.51 mmoles, 1 eq.) was dissolved in dry dichloromethane (25 ml) and piperidine (1.36 ml, 13.8 mmoles, 2.5 eq.) was added dropwise. The mixture was stirred for 4 h, followed by a purification by flash chromatography (SiO_2, *n*-hexane:EtOAc 20:80). The product was obtained as a colorless oil (0.8 g, 78% yield), which was immediately used in the next step.

^{1}H NMR (400 MHz, $CDCl_3$) δ 5.30 (s, 1H), 3.75 (d, $J = 1.3$ Hz, 3H), 3.57–3.45 (m, 1H), 2.50 (s, 2H), 2.14 (dq, $J = 13.6$, 7.2 Hz, 1H), 1.87 (dq, $J = 14.9$, 7.6 Hz, 1H), 1.55–1.78 (m, 2H).

2.1.4. Synthesis of compound 4

2,2′-dithiodipyridine (5 g, 22.7 mmoles, 1 eq.) was dissolved in methanol (70 ml) under inert atmosphere. 2-mercaptoethanol (1.6 ml, 22.7 mmoles, 1 eq.) was added dropwise over 10 min and the reaction was stirred for 2 h. The reaction mixture was purified by flash chromatography (SiO_2, *n*-hexane:EtOAc 60:40). The intermediate was obtained as a colorless oil (2.7 g, 64% yield).

^{1}H NMR (400 MHz, $CDCl_3$) δ 8.59 (ddd, $J = 5.0$, 1.8, 0.9 Hz, 1H), 7.67–7.61 (m, 1H), 7.46 (dt, $J = 8.2$, 1.1 Hz, 1H), 7.22 (ddd, $J = 7.5$, 5.0, 1.1 Hz, 1H), 3.88–3.81 (m, 2H), 3.04–2.97 (m, 2H).

The intermediate (1.1 g, 5.87 mmoles, 1 eq.) was dissolved in DCM (50 ml) and further reacted with 4-nitrophenyl chloroformate (1.3 g, 6.46 mmoles, 1.1 eq.) and triethylamine (1.63 ml, 11.7 mmoles, 2 eq.) for 4 h. Then the reaction mixture was concentrated and purified by flash chromatography (SiO_2, *n*-hexane:EtOAc 50:50). Compound 4 was obtained as a yellow oil (0.9 g, 44% yield).

^{1}H NMR (400 MHz, $CDCl_3$) δ 8.54 (dt, $J = 5.0$, 1.4 Hz, 2H), 8.33–8.24 (m, 4H), 7.76–7.67 (m, 4H), 7.42–7.34 (m, 4H), 7.19 (td, $J = 5.1$, 3.2 Hz, 2H), 4.57 (t, $J = 6.4$ Hz, 4H), 3.19 (t, $J = 6.4$ Hz, 4H).

2.1.5. Synthesis of compound 5 (redox-DON)

Compound 3 (800 mg, 4.3 mmoles, 1 eq.) was dissolved in dry dichloromethane (20 ml), followed by the addition of CP0330-01_cr (1.82 g, 5.16 mmoles, 1.2 eq.) and triethylamine (717 μl, 5.16 mmoles, 1.2 eq.). The mixture was stirred for 16 h at 23 °C, then washed with brine, dried over magnesium sulfate, concentrated and purified by flash chromatography (SiO_2, *n*-hexane:EtOAc 40:60). The product was obtained as a pale oil (0.64 g, 43% yield).

^{1}H NMR (400 MHz, $CDCl_3$) δ 8.48 (dt, $J = 4.7$, 1.4 Hz, 1H), 7.74–7.62 (m, 2H), 7.11 (ddd, $J = 6.8$, 4.9, 1.5 Hz, 1H), 5.49 (d, $J = 8.0$ Hz, 1H), 5.29 (s, 1H), 4.40–4.25 (m, 3H), 3.75 (s, 3H), 3.04 (t, $J = 6.4$ Hz, 2H), 2.42 (s, 2H), 2.28–2.15 (m, 1H), 1.99 (dt, $J = 14.5$, 7.4 Hz, 1H), 1.74 (s, 2H).

2.2. Characterization of redox-DON

2.2.1. NMR spectroscopy

All the NMR spectra were measured by the Bruker Avance III-400 spectrometer. The NMR spectra were measured at 295 K. The ^{1}H NMR spectra were measured at a proton frequency of 400.1 MHz and the ^{13}C NMR spectra at 100.8 MHz. To standardize the ^{1}H NMR spectra, the internal signal of DMSO-d_6 (δ 2.50) and for the ^{13}C NMR spectrum, the internal signal of DMSO-d_6 (δ39.52) were used. The spectra were analyzed with Mestre-Nova software. The chemical shifts are indicated in δ scale, and the coupling constants J are given in Hz.

^{1}H NMR (400 MHz, DMSO-d_6) δ 8.47–8.45 (m, 1H), 7.85–7.73 (m, 3H), 7.27–7.24 (m, 1H), 6.06 (s, 1H), 4.23–4.13 (m, 2H), 4.05–3.98 (m, 1H), 3.63 (s, 3H), 3.10–3.07(t, $J = 6.2$ Hz), 2.40 (m, 2H), 2.02–1.91 (m, 1H) 1.83–1.74 (m, 1H). Residual ethyl acetate and water.

^{13}C NMR (101 MHz, DMSO-d_6) δ 193.57, 172.45, 158.95, 155.80, 149.60, 137.84, 126.21, 121.27, 119.28, 61.85, 53.14, 51.93, 33.61, 25.78, 19.28.

2.2.2. LC-MS

Redox-DON was characterized by liquid chromatography and tandem mass spectrometry (LC − MS/MS). Briefly, redox-DON (10 μM) was spiked into 1:1 acetonitrile:water mixture. Samples were analyzed using Waters Acquity-I-UPLC Class system (Waters Corporation, Milford, MA, USA) coupled with a Waters Vion IMS-QTof Mass Spectrometer equipped with LockSpray (Leucine-enkephalin (200 pg/μl)). Analyses were performed on an ACQUITY UPLC® BEH C18 1.7 μm column, 2.1 mm × 50 mm (Waters) heated at 30 °C. The mobile phase was maintained at a flow rate of 0.4 ml/min and contained water (A), acetonitrile solution (B) both containing 0.1% formic acid. Over a 5 min total run, the gradient was: 0–0.2 min, 5% B; 0.2–3 min, 5–75% B; 3–4 min, 75–95% B; 4–4.1 min, 5% B and 4.1–5 min to re-equilibrate the system in initial conditions. The instrument was controlled by Waters UNIFI 1.9.4 (3.1.0, Waters Corporation, Milford, MA, USA). Injection volume was 5 μl. The instrument was operated in positive polarity, sensitivity mode (33,000 FWHM at 556.2766 *m/z*). Data was acquired in HDMSe mode with a scan time of 0.036 s. The recorded mass range was from 50 to 1200 m/z for both low and high energy spectra. The collision energy was ramped from 20 to 40 V. The cone voltage was set to 30 V, capillary voltage was set to 3 kV, source offset was set to 50 V. Source temperature was set to 120 °C and desolvation temperature set to 500 °C. Cone gas flow rate was set to 50 l/h and desolvation gas flow rate was set to 1000 l/h.

2.2.3. In vitro release study by ^{1}H NMR spectroscopy

For the *in vitro* release study, redox-DON (12.5 mmol, 1 equiv) was dissolved in DMSO-d_6. Then, 2-mercaptoethanol (25 mmol, 2 equiv) was added to the dissolved redox-DON and the reaction was monitored at rt. by ^{1}H NMR spectroscopy over time (5 min-8 days). All the NMR spectra were measured by the Bruker Avance III-400 spectrometer at 295 K.

2.2.4. DON release study in mouse plasma and bioanalysis by LC-MS/MS

For the DON release studies, mouse plasma was used. Redox-DON (10 μM) was spiked into the plasma matrix and incubated in a thermomixer at 37 °C. At predetermined times (0, 2 and 30 min) 100 μl of the mixture was aliquoted and cold methanol (250 μl) was added to extract DON from the plasma. The samples were vortexed and centrifuged at 16000*g* for 5 min for protein precipitation. The supernatant (200 μl) was added to a new tube and the remaining solvent was evaporated at 45 °C. Then, 0.2 M sodium bicarbonate buffer (50 μl, pH 9.0) and 10 mM of dabsyl chloride in acetone (100 μl) were added to the tube. For the derivatization, the mixture was vortexed and incubated at 60 °C for 15 min. Analyses of DON release were conducted on a Xevo G2-S QTOF mass spectrometer coupled to the Acquity UPLC Class Binary Solvent manager and BTN sample manager (Waters, Corporation, Milford, MA). The injection volume was 5 μl. Mass spectrometer detection was operated in positive ionization using the ZSpray™ dual-orthogonal multimode ESI/APCI/ESCi® source. The TOF mass spectra were acquired in the sensitive mode over the range of *m/z* 50–1200 at an acquisition rate of 0.036 s/spectra. The instrument was calibrated using a solution of sodium formate (0.01 mg/l in isopropanol/H2O 90:10). A mass accuracy better than 5 ppm was achieved using a Leucine Enkephalin solution as lock-mass (200 pg/μl in ACN/H2O (50,50)) infused continuously using the LockSpray source. Source settings were as follows: cone, 25 V; capillary, 3 kV, source temperature, 150 °C; desolvation temperature, 500 °C, cone gas, 10 L/h, desolvation gas, 500 L/h. Data were processed using MassLynx™ 4.1 software. The separation was achieved using an ACQUITY UPLC® BEH C18 1.7 μm column, 2.1 mm × 50 mm (Waters) heated at 30 °C The mobile phase was maintained at a flow rate of 0.4 ml/min and contained water (A), acetonitrile solution (B) both containing 0.1% formic acid. Over a 5 min total run, the gradient was: 0–0.2 min, 5% B; 0.2–3 min, 5–75% B; 3–4 min, 75–95% B; 4–4.1 min, 5% B and 4.1 to 5 to re-equilibrate the system in initial conditions.

Appearance of DON derived from redox-DON was measured by the peak area of the DON-dabsyl derivative.

2.3. Biological assays

2.3.1. Mice

Five-week-old female BALB/c (BALB/cByJ) mice were purchased from Charles River Laboratories and acclimatized in the École Polytechnique Fédérale de Lausanne (EPFL) Center of PhenoGenomics animal facility for one week before starting experiments. T-cell receptor (TCR)-transgenic Thy1.1$^+$ pmel-1 (Pmel) mice (B6.Cg-*Thy1*^{a}/Cy Tg (TcraTcrb)8Rest/J) and TCR transgenic OT-II mice (C57BL/6-Tg (TcraTcrb)425Cbn/Crl) were purchased from Jackson Laboratory and maintained in the animal facility of the CPG at EPFL. The mice were housed in the EPFL Center of PhenoGenomics and were kept in individually ventilated cages with up to five mice per cage, at 19–23 °C, with 45–65% humidity and with a twelve-hour light-dark cycle. Experimental procedures in mouse studies were approved by the Swiss authorities (Canton of Vaud, animal protocol ID 3533) and performed in accordance with the guidelines from the Center of PhenoGenomics of EPFL.

2.3.2. Cells and tumor models

CT26 mouse colorectal cancer cells, B16F10 mouse melanoma cell, 4T1 mouse breast cancer cells, SW480 and LS1034 human colorectal cancer cells, and SKBR-3 human breast cancer cells were originally acquired from the American Type Culture Collection (ATCC). MC38 murine colon adenocarcinoma was a gift from Irvine lab (MIT). The ovalbumin-expressing B16OVA melanoma cell line was a gift from Ho lab (University of Lausanne). CT26 and SKBR-3 cells were cultured in complete RPMI-1640 medium, GlutaMAX™ Supplement (Gibco™/Thermo Fisher Scientific) supplemented with fetal bovine serum (FBS) (10% *v*/v, Gibco™/Thermo Fisher Scientific), HEPES (1 M, pH range 7.2 to 7.5, 1% v/v, Gibco™/Thermo Fisher Scientific), penicillin/streptomycin (1% *v*/v, Gibco™/Thermo Fisher Scientific), sodium pyruvate (100 mM, 1% v/v, Gibco™/Thermo Fisher Scientific) and 2-mercaptoethanol (55 mM, 0.1% v/v, Gibco™/Thermo Fisher Scientific). LS1034 cells were cultured in complete RPMI-1640 medium, GlutaMAX™ Supplement (Gibco™/Thermo Fisher Scientific) supplemented with fetal bovine serum (FBS) (10% *v*/v, Gibco™/Thermo Fisher Scientific) and penicillin/streptomycin (1% *v*/v, Gibco™/Thermo Fisher Scientific). SW480 cells were cultured in complete Leibovitz's L-15 medium (Sigma-Alridch) supplemented with fetal bovine serum (FBS) (10% *v*/v, Gibco™/Thermo Fisher Scientific). B16F10 and B16OVA cells were cultured in complete DMEM, GlutaMAX™ Supplement (Gibco™/Thermo Fisher Scientific) supplemented with fetal bovine serum (FBS) (10% v/v, Gibco™/Thermo Fisher Scientific), HEPES (1 M, pH range 7.2 to 7.5, 1% v/v, Gibco™/Thermo Fisher Scientific), penicillin/streptomycin (1% v/v, Gibco™/Thermo Fisher Scientific), sodium pyruvate (100 mM, 1% v/v, Gibco™/Thermo Fisher Scientific) and 2-mercaptoethanol (55 mM, 0.1% v/v, Gibco™/Thermo Fisher Scientific). Cells were passaged every 2–3 days. For *in vivo* experiments, CT26 mouse colorectal cancer cells (3×10^5 or 5×10^5) were subcutaneously inoculated into the right flanks of BALB/c mice.

2.3.3. Tumor cell killing by DON prodrugs

B16F10 tumor cells were seeded at 10′000 cells/well in complete DMEM medium (200 µl/well) in a 96-well flat-bottom plate for 16 h. Then the stimuli-responsive DON-prodrug candidates, dissolved in DMSO, were added at concentrations between 0.1 and 100 µM to the adherent B16F10 cells (0.5% *v*/v). The cells were incubated with the prodrugs for 48 h at 37 °C, followed by the addition of 3-(4,5-dimethylthiazol-2-yl)-2,5- diphenyltetrazolium bromide (MTT) in PBS (5 mg/ml, 10 µl/well) for 4 h at 37 °C. The formed crystals were dissolved by adding isopropanol (100 µl/well) at 37 °C for 16 h. The absorbance was measured at 590 nm and the data was normalized to the controls. Cells were resuspended in FACS buffer, stained with 4′,6-diamidino-2-phenylindole (DAPI) and analyzed with flow cytometry.

2.3.4. Preparation of PMEL CD8$^+$ T cells

Spleens from PMEL mice were mechanically disrupted and ground through a 70-µm strainer (Fisher Scientific). Red blood cells (RBCs) were lysed with ACK lysis buffer (2 ml per spleen, Gibco™/Thermo Fisher Scientific) for 5 min at 23 °C. The splenocytes were washed twice with cold PBS (pH 7.4, Gibco™/Thermo Fisher Scientific), followed by resuspension at a cell density of 2×10^6 per ml in complete RPMI medium supplemented with mouse IL-2 (10 ng ml^{-1}, BioLegend) and IL-7 (2 ng ml^{-1}, BioLegend), as well as human gp100$_{25–33}$ (1 µM, GenScript). After two days of culture, live cells were enriched by density gradient centrifugation against Ficoll-Paque PLUS (GE Healthcare), followed by another two days of culture at a cell density of 0.5 to 1.0×10^6 per ml in complete RPMI medium supplemented with mouse IL-2 (10 ng ml^{-1}) and IL-7 (2 ng ml^{-1}) to afford activated CD8$^+$ T cells with purity >95% (validated by automated cell counter (Thermo Fisher Scientific) and flow cytometry analyses). The CD8$^+$ T cells were maintained in culture up to day 10 in complete RPMI medium supplemented with mouse IL-2 (10 ng ml^{-1}) and IL-7 (2 ng ml^{-1}) unless otherwise noted. Live cells were enriched by density gradient centrifugation against Ficoll-Paque PLUS before every experiment to a purity >95%.

2.3.5. Preparation of OTII CD4$^+$ T cells

Spleens from OTII mice were mechanically disrupted and ground through a 70-µm strainer (Fisher Scientific). Red blood cells (RBCs) were lysed with ACK lysis buffer (2 ml per spleen, Gibco™/Thermo Fisher Scientific) for 5 min at 23 °C. The splenocytes were washed twice with cold PBS (pH 7.4, Gibco™/Thermo Fisher Scientific), followed by resuspension at a cell density of 2×10^6 per ml in complete RPMI medium supplemented with mouse IL-2 (10 ng ml^{-1}, BioLegend) and IL-7 (10 ng ml^{-1}, BioLegend), as well as OVA$_{323–339}$ (1 µM, GenScript). After three days of culture, live cells were enriched by density gradient centrifugation against Ficoll-Paque PLUS (GE Healthcare), followed by another three days of culture at a cell density of 0.5 to 1.0×10^6 per ml in complete RPMI medium supplemented with mouse IL-2 (10 ng ml^{-1}) and IL-7 (10 ng ml^{-1}) to afford activated CD4$^+$ T cells with purity >95% (validated by automated cell counter (Thermo Fisher Scientific) and flow cytometry analyses). The CD4$^+$ T cells were maintained in culture up to day 10 in complete RPMI medium supplemented with mouse IL-2 (10 ng ml^{-1}) and IL-7 (10 ng ml^{-1}) unless otherwise noted. Live cells were enriched by density gradient centrifugation against Ficoll-Paque PLUS before every experiment to a purity >95%.

2.3.6. Preparation of bone marrow-derived dendritic cells (BMDC)

Femur and tibia bones of mice were cleaned from skin and flesh. The bones were placed into 70% ethanol for 2 min and then into cold PBS. The epiphysis of the bones was cut off and the shafts were flushed with PBS using a 5 ml syringe topped with a 23 g needle until all the red marrow came out. The monocytes were obtained as a suspension by a passage through the 23 g needle and filtration through a 70-µm strainer (Fisher Scientific). Red blood cells (RBCs) were lysed with ACK lysis buffer (2 ml per spleen, Gibco™/Thermo Fisher Scientific) for 5 min at 23 °C. The monocytes were cultured in complete RPMI medium supplemented with 20 ng/ml GM-CSF at a cell density of 0.4×10^6 per ml. After 3 days the medium was replaced. The suspension cells were harvested on day 8 for cell assays.

2.3.7. Preparation of bone marrow-derived macrophages (BMDM)

Femur and tibia bones of mice were cleaned from skin and flesh. The bones were placed into 70% ethanol for 2 min and then into cold PBS. The epiphysis of the bones was cut off and the shafts were flushed with PBS using a 5 ml syringe and a 23 g needle until all the red marrow came out. The monocytes were obtained as a suspension by a passage through the 23 g needle and filtration through a 70-µm strainer (Fisher Scientific). Red blood cells (RBCs) were lysed with ACK lysis buffer (2 ml per

spleen, Gibco™/Thermo Fisher Scientific) for 5 min at 23 °C. The monocytes were cultured in complete DMEM medium supplemented with 5% horse serum and 20% L929-derived culture medium containing M-CSF at a cell density of 0.4×10^6 per ml. After 4 days the medium was replaced. The adherent cells were harvested on day 8 for cell assays.

2.3.8. Peripheral blood mononuclear cells (PBMC)-derived human CD8+ T cells

Frozen aliquots of human PBMCs from anonymous healthy donors (prepared as buffy coats) were used. After gentle thawing, the PBMCs were incubated in complete RPMI medium for 1 h at 37 °C. Human $CD8^+$ T cells were then isolated by magnetic-activated cell sorting (MACS) using a human $CD8^+$ T cell isolation kit (Miltenyi Biotec). The CD8+ enriched T cells were resuspended at a cell density of 1×10^6 per ml in complete RPMI medium and activated by Gibco™ Dynabeads™Human T-Activator CD3/CD28 for T Cell Expansion and Activation (Fisher Scientific) at a dynabeads to cell ratio of 1:1. The T cells were then supplemented with human IL-2 (50 IU ml^{-1}) and human IL-15 (1 ng/ml) and cultured for 3 days at a cell density of 1×10^6 per ml in complete RPMI. After 3 days of culture, the dynabeads were removed by placing the cell suspension on a magnet for 1–2 min. The T cells were then rested for another 4 days at cell density of 0.5 to 1.0×10^6 per ml in complete RPMI medium supplemented with IL-2 (30 IU ml^{-1}) to afford activated human $CD8^+$ T cells with purity >92% (validated by automated cell counter (Thermo Fisher Scientific) and flow cytometry analyses).

2.3.9. Proliferation of Pmel $CD8^+$ T cells and other immune cells in the presence of DON prodrugs

Pmel $CD8^+$ T cells (day 4 after activation) in a round-bottom 96-well plate (50′000 cells/well) were suspended in complete RPMI medium (200 μl/well) supplemented with recombinant mouse IL2 (10 ng/ml) and DON prodrug candidates at concentrations between 0.1 and 100 μM. The cells were incubated for 48 h at 37 °C, followed by staining with DAPI and flow cytometry analysis. Other immune cells were seeded at equivalent densities in adequate well plates (96-wells for $CD8^+$, $CD4^+$ T cells and BMDC, 12-well plates for BMDM).

2.3.10. In vitro co-culture of T cells and tumor cells

B16F10 and B16OVA tumor cells were cultured in complete DMEM as described above. Collected B16F10 and B16OVA tumor cells (1.5×10^4/well) were seeded in 96-well microplates in complete RPMI medium (described above) at 37 °C for 16 h. Following aspiration of tumor culture medium, activated PMEL $CD8^+$ T cells or OT-II $CD4^+$ T cells (3×10^3/well or 1.5×10^4/well) on day 4 after activation as described above were suspended in complete RPMI medium supplemented with IL-2 (10 ng ml^{-1}) and added to the tumor cell culture at a T cell/tumor cell ratio of 1:1 or 1:5. After another two days of coculture, $CD8^+$ and $CD4^+$ T cells were analyzed in flow cytometry analyses. To determine the lysis of target cells, the viability of tumor cells from the coculture was measured with DAPI staining and flow cytometry.

2.3.11. Antitumor therapy experiments

Mice bearing established tumors with areas around 20–50 mm^2 (day 5 post inoculation or as indicated) received DON prodrug (1 mg/kg/dose, s.c.) or vehicle (30% propylene glycol in PBS) treatments daily on days 5–9 and lower doses of DON prodrugs (0.3 mg/kg/dose, s.c.) on days 10–15 post tumor inoculation unless otherwise noted. Tumor area and body weight were measured every other day. Tumor area was calculated by the formula Area = Length × Width from caliper measurements of two orthogonal diameters. Mice were euthanized when body weight loss was beyond 15% of predosing weight, or tumor area reached 150 mm^2 (as a predetermined endpoint).

2.3.12. Combination therapy of DON prodrugs with checkpoint inhibitors

Mice bearing established tumors with areas around 20–50 mm^2 (day 5 post inoculation or as indicated) received checkpoint inhibitors anti-PD1 (200 μg/mouse/dose, s.c.) and anti-CTLA-4 (100 μg/mouse/dose, s.c.) or PBS control on days 5, 7 and 9 and DON prodrug (1 mg/kg/dose, s.c.) or vehicle (30% propylene glycol in PBS) treatments daily on days 5–9 and lower doses of DON prodrugs (0.3 mg/kg/dose, s.c.) on days 10–15 post tumor inoculation unless otherwise noted. Tumor area and body weight were measured every other day. Tumor area was calculated by the formula Area = Length × Width from caliper measurements of two orthogonal diameters. Mice were euthanized when body weight loss was beyond 15% of predosing weight, or tumor area reached 150 mm^2 (as a predetermined endpoint). In tumor cell rechallenging experiments 3×10^5 CT26 tumor cells were re-implanted subcutaneously into the left flanks of the surviving mice from treatment groups at day 90 post primary inoculation. Age-matched BALB/c mice were subcutaneously inoculated with the same number of tumor cells as the control. Survival of rechallenged mice was monitored for at least another 60 days.

2.3.13. Analyses of immune cells in tumors and spleens

BALB/c mice were inoculated subcutaneously with CT26 tumor cells (5×10^6) and received checkpoint inhibitors or PBS control subcutaneously (s.c) in three doses and DON prodrug or vehicle s.c. treatments in ten doses starting on day 5 post tumor inoculation. On day 14 (or as indicated), tumors were dissected from the surrounding tissues, weighed, mechanically minced and stirred at 1000 r.p.m. in RPMI-1640 medium with collagenase Type IV (1 mg ml^{-1}, Gibco/Thermo Fisher Scientific), dispase II (100 μg ml^{-1}, Sigma-Aldrich), hyaluronidase (100 μg ml^{-1}, Sigma-Aldrich) and DNase I (100 μg ml^{-1}, Sigma-Aldrich) at 37 °C for 60 min for digestion. RBC lysis was performed on the digested tumor samples with ACK lysing buffer. The tumor samples were washed with FACS buffer (cold PBS with BSA albumin (0.2%, wt/v, Sigma-Aldrich)) and filtered through 70-μm strainers. Tumor-infiltrating leukocytes were then enriched by density gradient centrifugation against Percoll (GE Healthcare), resuspended in FACS buffer, stained with indicated antibodies and analyzed with flow cytometry.

2.3.14. Histology analysis

Mice were sacrificed at the respective endpoints. Spleens, colons and livers were collected and stored in 4% PFA in PBS solution and packaged in histology cassettes. After a total of 48 h of incubation in 4% PFA in PBS, the cassettes were washed and transferred into PBS. The samples were paraffin perfused, embedded into paraffin blocks and cut to 4 mm tissue slices with a microtome. The tissue slices were loaded on slides and stained with hematoxylin and eosin for analysis.

2.3.15. Measurement of liver enzymes in serum

For serum biochemistry, blood samples (200 μl) were collected in Serum Gel CAT tubes (Microvette® 500, Sarstedt AG) from inferior vena cava of the mice immediately after euthanasia. The serum was isolated after centrifugation at +4 °C and then stored at −80 °C.

Serum parameters were measured on 2 times diluted samples (1,1 ratio of serum to diluent) using Dimension®Xpand Plus (Siemens Healthcare Diagnostics AG, Dudingen, Switzerland). The biochemical tests were performed according to the manufacturer kit for each parameter, including transaminase ASAT (Siemens Healthcare, DF41A) and transaminase ALT (Siemens Healthcare, DF143).

2.3.16. Flow cytometry analyses

For surface marker staining, cells were collected in U-bottom 96-well plates (Thermal Fischer Scientific), blocked with anti-mouse CD16/32 antibody (BioLegend) and incubated with indicated antibodies at 4 °C for 20 min, followed by live/dead staining by DAPI (Sigma-Aldrich) or Zombie Aqua Fixable Dye (BioLegend). Cells were then washed with FACS buffer and resuspended in the same buffer for flow cytometry analyses. For intracellular cytokine staining, cells were first stimulated by a Cell Stimulation Cocktail (protein transport inhibitors included, Invitrogen/Thermo Fisher Scientific) at 37 °C for 4–6 h. Then cells were first stained for surface markers and Aqua Fixable Dye as described

above. Next, cells were fixed and permeabilized with a Cytofix/Cytoperm Fixation/Permeabilization Solution Kit (BD Biosciences) for cytokine staining or a Foxp3/Transcription Factor Staining Buffer Set (eBioscience) for transcription factors staining following the manufacturer's instructions. Intracellular staining was performed by incubation with the respective antibodies. Cells were then washed with buffers from the fixation/permeabilization kits and resuspended in the same buffers for flow cytometry analyses. Data was collected using an Attune NxT Flow Cytometer with Attune NxT Software v.3 (Invitrogen/Thermal Fischer Scientific). Analyses were performed using FlowJo™ 10.8.0 (BD Life Sciences). Gate margins were determined by isotype controls and fluorescence-minus-one controls.

2.3.17. Antibodies and reagents for flow cytometry

The following antibodies or staining reagents were purchased from BioLegend: CD16/32 (93, 101302), CD45 (QA17A26, 157605; 30-F11, 103139), CD8α (53–6.7, 100714), CD8β (YTS256.7.7, 126606; YTS156.7.7, 126633), CD4 (RM4–5, 100526, 100543), CD11b (M1/70, 101228, 101208), CD11c (N418, 117348, 117307), CD19 (6D5, 115520), F4/80 (BM8,123108), I-A/I-E (MHC-II, M5/114.15.2, 107643), NKp46 (29A1.4, 137630), NK1.1 (PK136, 108739, 108707), CD19 (6D5,115520), CD80 (16-10A1, 104714), CD86 (GL-1, 105037), Gr-1 (RB6-8C5, 108424, 108408, 108405), CD44 (IM7, 103006, 103028), CD69 (H1.2F3, 104512, 104514), PD-1 (29F.1A12, 135216, 135205), Foxp3 (MF-14, 126406), Ki67 (16 A8, 652424), T-bet (4B10, 644828), IL-4 (11B11, 504133), Granzyme B (GB11, 515403), IFN-γ (XMG1.2, 505826), TNF-α (MP6-XT22, 506308, 506306), IL-2 (JES6-5H4, 503822), CD117 (c-Kit, 2B8, 105824), CD3 (17A2, 100206), CD25 (PC61, 102024), CD62L (MEL-14, 104408, 104432), Ly-6A/E (Sca-1, D7, 108105), CD122 (5H4, 105906), TER-119 (TER-119, 116208), B220 (RA3-6B2, 103207), Ly-6C (HK1.4, 128026), CD163 (S15049F, 156703), CD206 (C068C2, 141719).

2.3.18. Statistical analysis

Statistical analysis was performed using GraphPad Prism (GraphPad Software, Version 9.4.0). Data are presented as mean ± s.e.m. unless otherwise indicated. Comparisons of two groups were performed by using two-tailed unpaired Student's *t*-test. Comparisons of multiple groups at a single time point were performed by using one-way analysis of variance (ANOVA). Survival data were analyzed using the Kaplan-Meier log-rank test. No statistically significant differences were considered when *P* values were larger than 0.05.

3. Results

3.1. Design, synthesis, and characterizations of redox-DON

Scheme 1 illustrates our rationale for designing a novel redox-responsive DON prodrug. The parent molecule DON had been reported to cause side effects in patients, among them severe nausea, vomiting, mucositis, hepatic encephalopathy and myelosuppression [28]. We hypothesized that we would increase the safety of previously reported DON prodrugs that bore enzymatically cleavable moieties [20], such as JHU083, by designing a prodrug in response to the reducing condition, a chemical characteristic of the TME. We chose to use 2-(pyridin-2-yldisulfaneyl)ethyl carbamate as the redox-responsive moiety for the redox-DON due to the minimal modification of the parent drug DON and the easy installability from the unstable common intermediate of previously reported DON prodrugs [20]. Redox-DON was synthesized in four steps from N and C-terminal-protected glutamic acid (Fig. S1). At the N-terminus we started with a base-cleavable fluorenylmethoxycarbonyl (Fmoc) group, at the C-terminus we used a methyl group which is present in the final molecule as a methyl ester. First the glutamic acid side chain was activated to generate a cyclic intermediate, followed by the installation of the diazomethane moiety as previously reported [20]. This step required profound chemical expertise due to the use of the highly reactive trimethylsilane-diazomethane reagent. Next, the N-term protection group Fmoc was cleaved to form the unstable intermediate, C-term-protected DON, which was subsequently coupled to the redox-responsive pro-group to yield redox-DON. The structure of the final redox-DON molecule is composed of DON at the core, an esterase-cleavable C-terminal methyl ester and a redox-responsive N-terminal disulfide linker. The structure of redox-DON was confirmed by proton (^{1}H) and carbon (^{13}C) nuclear magnetic resonance (NMR) (Fig. 1A and B).

Next, we investigated the redox responsiveness of redox-DON when exposed to mouse plasma. Upon reaction with reducing thiols in the TME or glutathione in the cytoplasm of cells, the linker was designed to release DON in the tumor, leaving no traces of the redox-modification. Redox-DON and DON released from its pro-moieties were investigated by ultra-performance liquid chromatography – tandem mass spectrometry (UPLC-MS/MS) (Fig. 1C, Fig. S2A—B). Due to the instability of DON and the difficulty to detect DON in complex matrices, we derivatized released DON with dabsyl chloride for detection [20,29]. We observed the molecular peak of the DON-derivative shortly after the exposure and thereby confirmed that the parental drug DON was released from redox-DON in a matrix that mimics *in vivo* conditions. Furthermore, redox-DON was exposed to different thiol-containing reducing agents including 2-mercaptoethanol (2-ME), 1,4-dithiothreitol (DTT), glutathione (GSH) in deuterated dimethyl sulfoxide/water (DMSO-d_6/D_2O) mixtures, to further reveal the releasing mechanism by ^{1}H NMR. The reducing agents reacted with the disulfide bond of redox-DON in a thiol-disulfide exchange reaction to from new disulfide species with the previous redox-DON which we termed intermediates (Fig. S3A). We observed that these intermediates were stable over prolonged time (Fig. S3B), indicating that DON release from redox-DON in mouse plasma as described above was likely subject to a mixture of reducing and enzymatic *in vivo* conditions.

3.2. Redox-DON shows equivalent antitumor efficacy and enhanced safety in comparison to the state-of-the-art DON prodrug JHU083

Despite glutamine being an unessential amino acid, different tumors have been reported to be glutamine addicted and sensitive to glutamine inhibition [30]. We set out to evaluate the extent of dependence on glutamine metabolism in the context of different cancer cell lines treated by DON prodrugs. The influence on the growth of all investigated cell lines, including mouse colon carcinoma CT26 and MC38, melanoma B16F10, and mammary carcinoma 4T1, was tested in a dose-dependent manner mediated by both DON prodrugs, redox-DON and JHU083 (Fig. 2A-D), showing potent cell growth inhibition when concentrations were above 10 nM. The corresponding effective concentrations at half maximum (EC_{50}) were derived from the dose-response curves (Fig. 2E). In all the tested cell lines, redox-DON and JHU083 exhibited similar EC_{50} values, suggesting both prodrugs possess equivalent cytotoxicity against different cancer cell lines. A similar trend was observed in human colorectal carcinoma cell lines SW480 and LS1034, as well as human breast cancer line SKBR-3 (Fig. S4A—C). The trend of equivalently low EC_{50} of these DON prodrugs against various cancer cell lines was confirmed in repeated experiments.

Human colon carcinoma has shown sensitivity towards glutamine restriction in preclinical models [9,18]. We chose the CT26 tumor cell line with an EC_{50} value of 37 and 30 nM for JHU083 and redox-DON, respectively, for further *in vivo* evaluation. We treated BALB/c mice bearing subcutaneous CT26 tumors according to the dosing schedule reported for JHU083 [12]. Mice received vehicle, JHU083, or redox-DON over the course of 15 days. For the first five days, the mice received 67 nmol per injection (1× dose) of DON prodrugs, followed by 10 days of 20 nmol per injection (0.3× dose) to avoid lethal toxicities (Fig. 2F). Initially, both DON prodrugs could control tumor growth; concurrently with the withdrawal of treatment, however, the tumors grew fast to the endpoint in both treatment groups (Fig. 2G). There were

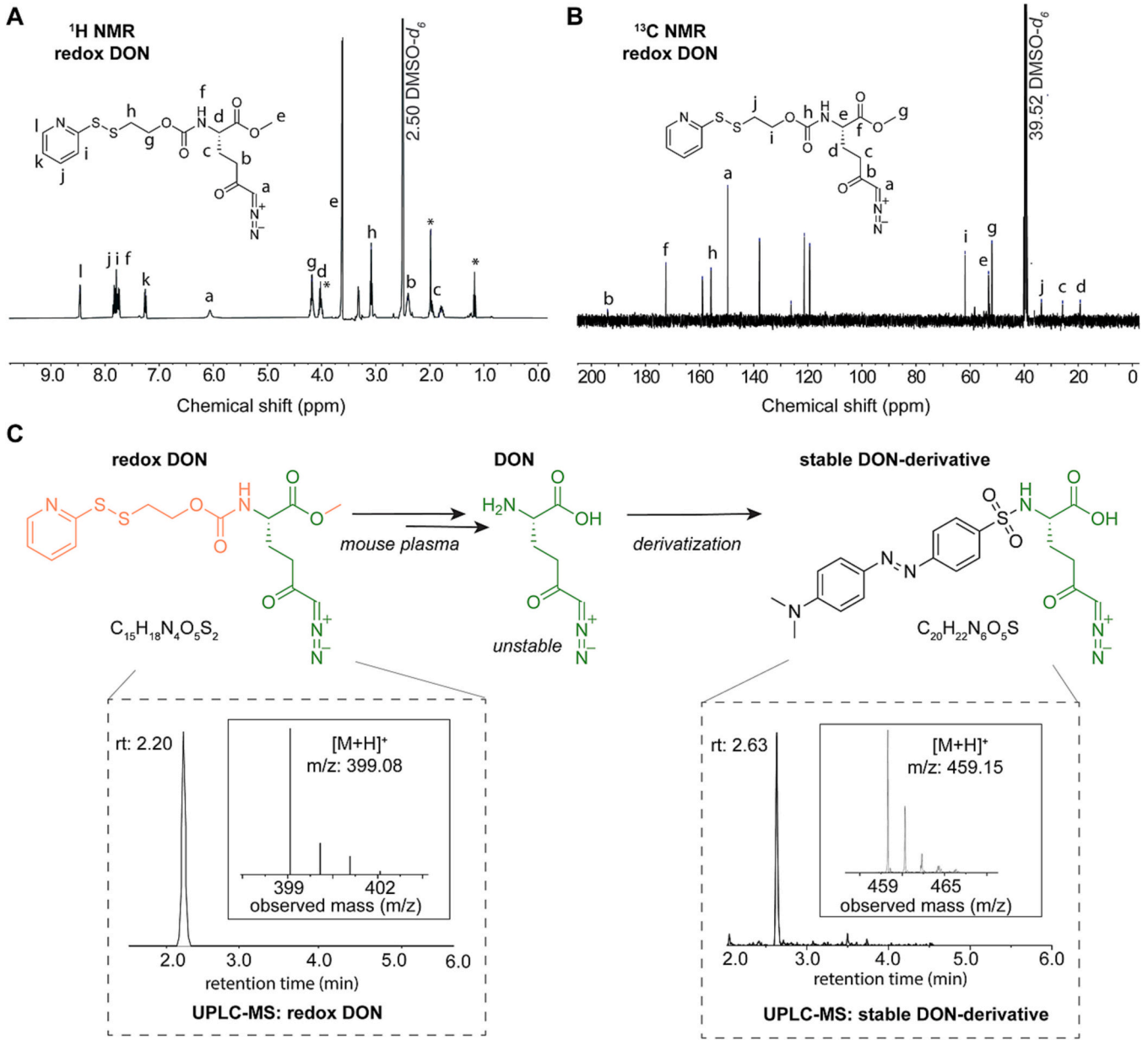

Fig. 1. Characterization and release study of redox-DON. The structure of redox-DON was confirmed by ^{1}H NMR (400 MHz) (A) and ^{13}C NMR (100 MHz) (B) acquired in DMSO-d_6. (C) Schematic illustration of redox-DON exposure in mouse plasma and subsequent derivatization for the detection by UPLC-MS/MS. Redox-DON was spiked into plasma and the released DON was quickly extracted at 2 min and derivatized with dabsyl chloride. Substrate and product were observed at the respective $[M + H]^+$ ion peaks for redox-DON (399.08) and the dabsyl-DON-derivative (459.15). Asterisks (*) labels are the residual solvent peaks corresponding to ethyl acetate.

no noticeable differences between JHU083 and redox-DON-treated groups in tumor growth and survival (Fig. 2G and H). Despite the different responsiveness, the *in vivo* anti-cancer efficacy was equivalent for both prodrugs in the CT26 tumor model.

Surprisingly, we observed a marked deviation of the body weight development between JHU083 and redox-DON-treated mice (Fig. 2I and J). Particularly, on days 12 and 18 of the treatment there were noteworthy drops in average body weight in the group of mice receiving JHU083 but not the group of mice treated with redox-DON, suggesting an improved safety profile of redox-DON as compared to JHU083. The body weight drops occurred with increasing accumulated dose of the administered JHU083 indicating likely a chronic toxicity. We hypothesized that the origin of toxicity of JHU083 could be related to adverse effects observed in human trials with the parent drug DON, which was ameliorated in the prodrug of redox-DON.

3.3. Redox-DON mitigates the systemic toxicities in spleen and gastrointestinal tract

Next, we investigated and compared the toxicity of JHU083 and redox-DON in a dose-escalation study in mice [12]. BALB/c mice bearing CT26 tumors were treated with daily injections of vehicle, JHU083, and redox-DON at doses of 67 (1× dose) or 200 (3× dose) nmol, respectively, from day 9 post inoculation (Fig. 3A). After six injections, the mice treated with JHU083 at high dose (200 nmol) reached an average of 15% body weight loss, the predetermined endpoint to sacrifice the mice, while the mice receiving redox-DON at the same high dose (200 nmol) showed noticeably less body weight loss (10%) (Fig. 3B). At low dose (67 nmol), treatment with redox-DON showed no toxicity as compared to the vehicle-treated group, whereas JHU083 caused 7% body weight drop even at the low dose (67 nmol). This trend

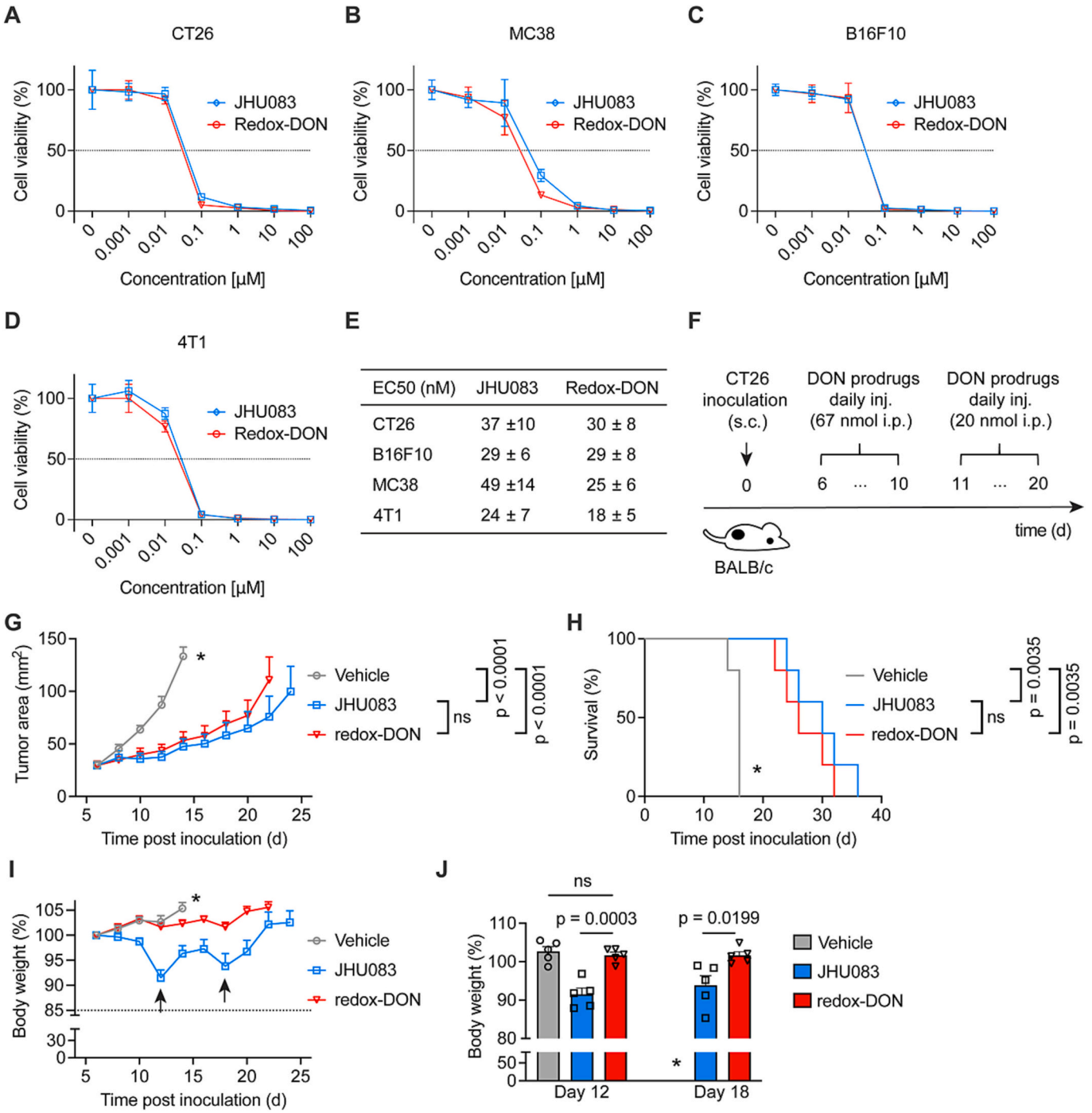

Fig. 2. Redox-DON shows equivalent antitumor efficacy and enhanced safety in comparison to JHU083. (A-D) Representative dose-response curves of DON prodrug-treated tumor cells including CT26 (A), MC38 (B), B16F10 (C) and 4T1 (D). Cell viability was normalized to vehicle-treated cells ($n = 3$). The error bars present the data as mean ± s.e.m. All experiments were performed at least twice. (E) EC_{50} values (mean ± s.e.m) derived from dose-response curves in (A-D) to compare cytotoxicity of JHU083 and redox-DON *in vitro*. (F-J) BALB/c mice were inoculated subcutaneously with CT26 tumor cells (0.5×10^6) and received daily intraperitoneal (i.p.) injections of vehicle, JHU083 or redox-DON from day 6 until day 20 with indicated doses ($n = 5$ mice). Shown is the schematic illustration of treatment schedule (F), average tumor growth curves (G), survival curves (H), and average body weight curves (observed body weight drops are indicated with arrows) (I). The average body weights in the different groups were compared on day 12 and day 18 (J). *All mice in the vehicle-treated group reached the endpoint between day 12 and 14 post tumor inoculation.

manifested also in individual body weight curves (Fig. S5A). No significant difference in body weight drops between the high dose redox-DON (200 nmol) and the low dose JHU083 (67 nmol) was observed, indicating that a three times higher dose of redox-DON could be applied, leading to the same adverse effects as the standard dose of JHU083. It is worth mentioning that in all treatment groups, the tumor growth was significantly inhibited compared to the vehicle-treated group, suggesting the doses were effective therapeutically (Fig. S5B). No correlation between tumor growth and body weight drop could be noted.

To examine potential toxicities in vital organs, on day 15 post tumor inoculation, we sacrificed the mice and collected spleen and colon tissues for flow cytometry and histopathological analyses. While treatment

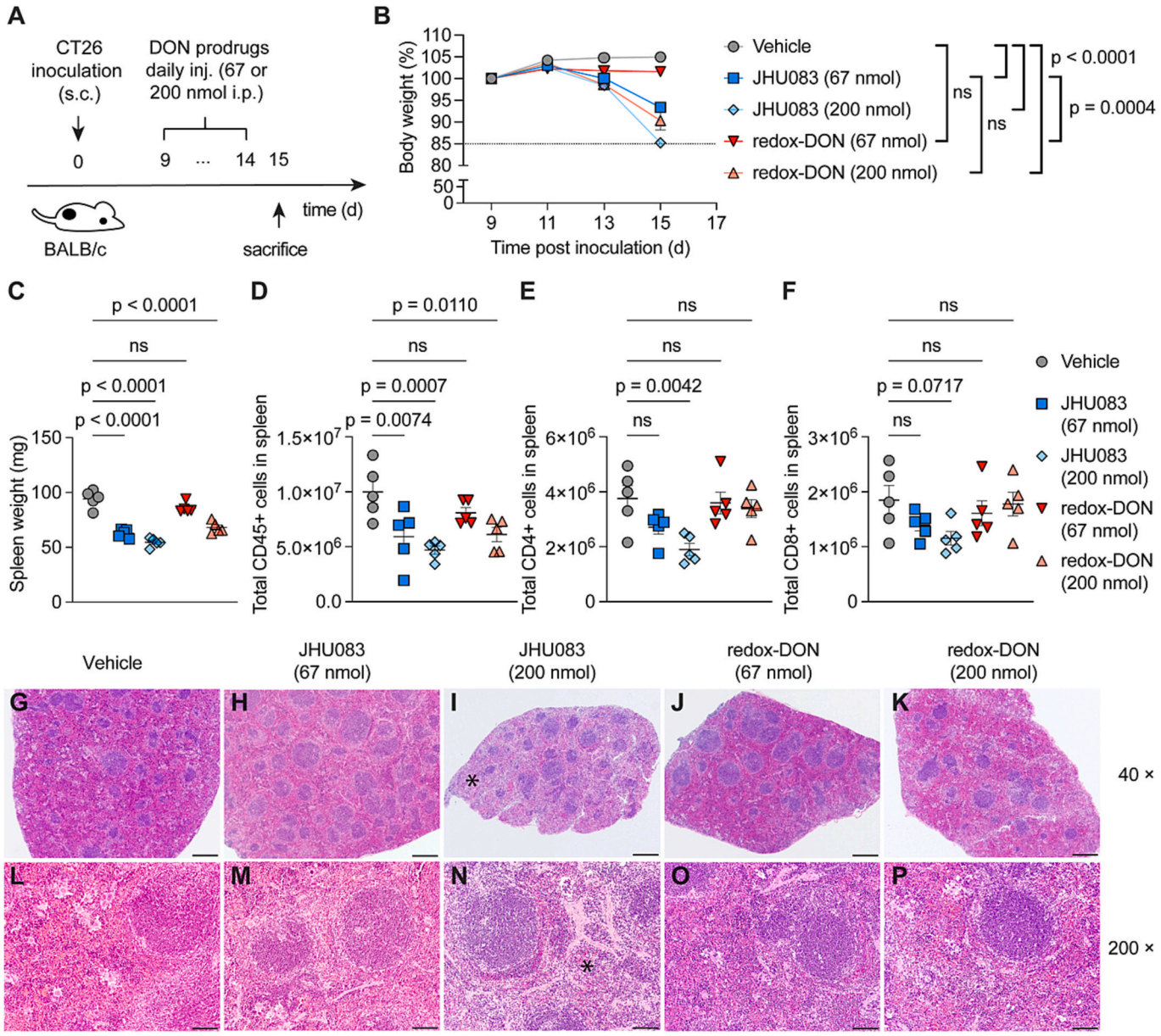

Fig. 3. Redox-DON reduces the toxicity of DON-prodrug glutamine inhibition in the spleen. (A-F) BALB/c mice bearing CT26 tumors were administered daily i.p. injections over six days of vehicle, 67 nmol or 200 nmol of JHU083 and redox-DON, respectively. Mice were euthanized on day 15, and the tissues were processed for histopathological and flow cytometry analyses ($n = 5$ mice). Shown are the schematic illustration of treatment schedule (A), average body weight curves (B), spleen weight (C), total counts of CD45+ lymphocytes (D), $CD4^+$ T cells (E) and $CD8^+$ T cells (F). (G-P) are H&*E*-stained spleen tissue sections of representative individuals from the different treatment groups. (G-K) are spleen images at low power field magnification (40×), (L-P) at high (200×) magnification of vehicle- (G, L), JHU083 (67 nmol)- (H, M), JHU083 (200 nmol)- (I, N), redox-DON (67 nmol)- (J, O) and redox-DON (200 nmol)-treated (K, P) mice. Asterisks (*) indicate areas of reduced red pulp. Scale bar 500 μm (G-K), 100 μm (L-P). (For interpretation of the references to colour in this figure legend, the reader is referred to the web version of this article.)

with low-dose redox-DON (67 nmol) exhibited no overt toxicities in the spleen, low and high-dose JHU083 (67 and 200 nmol) and high-dose redox-DON (200 nmol) induced marked decrease in spleen weight as well as total counts of $CD45^+$ lymphocytes (Fig. 3C-D). Total counts of $CD8^+$ and $CD4^+$ T cells were reduced in the high-dose JHU083 (200 nmol) treated group (Fig. 3E-F). This suggests at the low dose (67 nmol), JHU083 but not redox-DON induced toxicity towards the spleen.

The morphological impact of the different treatments was compared in tissue sections from the spleen stained with hematoxylin and eosin (H&E) for analysis. White and red pulp were present in all tissue sections (Fig. 3G-K). The red pulp was largely extended by extramedullary hematopoiesis (EMH) of all cell lineages, activation of B-lymphocytes presented in follicles within geminal centers of the white pulp (Fig. 3L-P). Only in the high-dose JHU083 (200 nmol)-treated group, the red pulp surface area was clearly reduced due to decreased EMH, suggesting severe adverse effects of the treatment. We therefore deduced that the size shrinkage of spleens was not only due to toxicity towards $CD45^+$ lymphocytes, but also due to decreased areas of erythroid and myeloid progenitor cell maturation.

The parental DON drug has been reported to cause gastrointestinal toxicities [28]. Therefore, we examined potential toxicities in colons by characterizing the length of the colons, as a measure of inflammation, and performing tissue level histopathological analysis, which are common procedures in models of colitis [31,32]. The average colon length was considerably decreased in mice treated with JHU083 at both low and high doses in comparison to the vehicle (Fig. 4A). However,

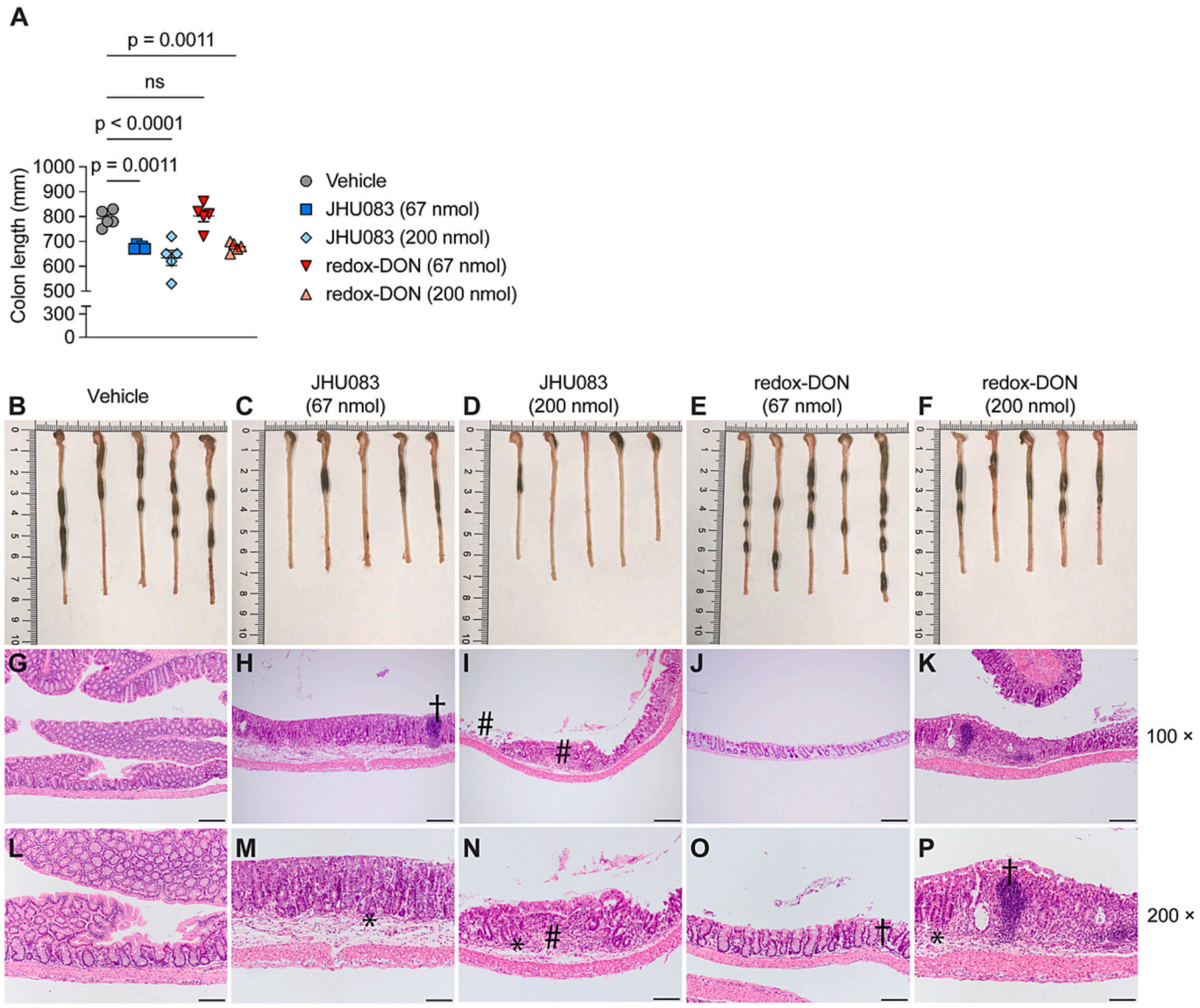

Fig. 4. Redox-DON reduces the toxicity of DON-prodrug glutamine inhibition in the colon. BALB/c mice bearing CT26 tumors were administered daily with i.p. injections over six days of vehicle, 67 nmol or 200 nmol of JHU083 and redox-DON, respectively. Mice were euthanized on day 15 for the analysis of the colons ($n = 5$ mice). Depicted are the average colon length (A), individual colons and their lengths after treatment with vehicle (B), JHU083 (67 nmol) (C), JHU083 (200 nmol) (D), redox-DON (67 nmol) (E), redox-DON (200 nmol) (F). (G-P) H&E-stained longitudinal sections of proximal colons of representative individuals from the different treatment groups. (G-P) are colon images at high power field 100× magnification and 200× magnification from vehicle- (G, L), JHU083 (67 nmol)- (H, M), JHU083 (200 nmol)- (I, N), redox-DON (67 nmol)- (J, O), and redox-DON (200 nmol)-treated (K, P) mice. Daggers (†) indicate lymph follicles in the mucosa; asterisks (*) indicate areas of edematous submucosa; hashtags (#) depict areas of ulceration and fibrosis. Scale bar 200 μm (G-K), 100 μm (L-P).

treatment with redox-DON at low dose (67 nmol) showed no impact on the colon length. In comparison to vehicle and redox-DON-treated mice, colons from mice treated with JHU083 at low and high doses contained less compacted feces, suggesting inflammation and digestive problems (Fig. 4B-F). Further histological analysis of H&*E*-stained proximal colon sections revealed different levels of immune cell infiltration in mucosa and submucosa as well as damages to mucosal crypts in treated groups (Fig. 4G-P). While the low dose redox-DON (67 nmol)-treated mice showed a mild increase of lymphocytes and plasma cells in the mucosa, low dose JHU083 (67 nmol)-treated mice presented mucosal lymph follicles and single cell necrosis of epithelial cells as well as elongated, tortured crypts with multiple mitotic figures and suggesting a stage of regeneration. Moreover, the submucosa was edematous supporting an ongoing inflammatory process. In high-dose redox-DON- and JHU083-treated mice (200 nmol), we observed multiple chronic ulcers, characterized by loss of the epithelial layer and underlying crypts and replacement of these structures by fibrosis and inflammatory cells.

Further, we investigated possible toxicities in the liver. We measured the activity of the liver enzymes alanine aminotransferase (ALT) and aspartate aminotransferase (AST) in the serum of mice from the different treatment groups. We did not observe any significant changes in the ALT/AST ratios (Fig. S5C). Moreover, H&*E*-stained liver tissue sections did not show any signs of toxicity in the treated mice (Fig. S5D—H).

3.4. *Redox-DON synergizes with checkpoint blockade antibodies for cancer treatment*

We next set out to test the influence of glutamine inhibition towards various immune cells *in vitro*. Both prodrugs, JHU083 and redox-DON, showed similar dose-dependent toxicities towards immune cells *in vitro*, including mouse and human $CD8^+$ T cells, mouse $CD4^+$ T cells, bone-marrow derived macrophages (BMDMs) and bone-marrow derived

dendritic cells (BMDCs) (Fig. S6A-E). Noticeably, the EC_{50} values of immune cells are 10–400-fold higher than those of cancer cell lines tested above (Fig. 5A and Fig. 2E), indicating much higher tolerance of glutamine restriction in immune cells than cancer cells. Interestingly, at concentrations below 1 μM, the DON prodrugs promoted the expansion of $CD8^+$ and $CD4^+$ T cells co-cultured with target cells (Fig. 5B, Fig. S6F-G). Together, the *in vitro* results suggest that glutamine restriction may be used in combination with immunotherapies for cancer.

Glutamine inhibitors combined with immune checkpoint blockade (ICB), such as antibodies that block programmed cell death protein 1 (PD1) or cytotoxic T lymphocyte associated protein 4 (CTLA-4), have shown some promise in preclinical models [12,13]. We therefore next tested the synergistic effects of redox-DON with checkpoint blockades. We compared four treatment groups, vehicle, redox-DON, ICB (anti-PD1 and anti-CTLA-4), and ICB + redox-DON (Fig. 5C). At the beginning, redox-DON alone showed a certain level of tumor control but eventually failed to exhibit long term efficacy (Fig. 5D). Starting from day 15 post tumor inoculation, we could observe the action onset of the treatment of ICB alone or ICB plus redox-DON, both leading to durable tumor growth control and long-term responses in 40% and 60% of treated mice, respectively (Fig. 5E). The combination of ICB and redox-DON exhibited the most potent anti-tumor efficacy. Noticeably, all the treated mice did not experience any body weight drop, suggesting low or none systemic toxicities (Fig. 5F). Further, the tumor-free mice from the group treated by ICB + redox-DON all rejected a rechallenge with CT26 tumor cells (Fig. S7), suggesting that glutamine restriction together with ICB may elicit long term anti-cancer immune memory responses that prevents relapses.

3.5. Redox-DON increases immune cell infiltration in the tumor

To investigate how redox-DON may impact immune cell infiltrates in tumor, we treated the mice the same way as above but collected all the tumor tissues for profiling infiltrating immune cells. The time point of the sacrifice was chosen at the tumor size-dependent endpoint of the group of vehicle-treated mice, which coincides with the onset of effects from the ICB treatment. We found the total number of leucocytes ($CD45^+$) in the tumor were increased in all treatment groups as compared to the vehicle group, but only to a statistically significant extent in the combination group of redox-DON plus ICB (Fig. 6A). Interestingly, the count of $CD4^+$ T cells was markedly increased in the redox-DON only and the combination group as compared to the vehicle group (Fig. 6B). Importantly, redox-DON plus ICB enhanced mostly the expansion of effector $CD4^+$ T cells (Teff, $Foxp3^-$ among $CD4^+$ T cells)

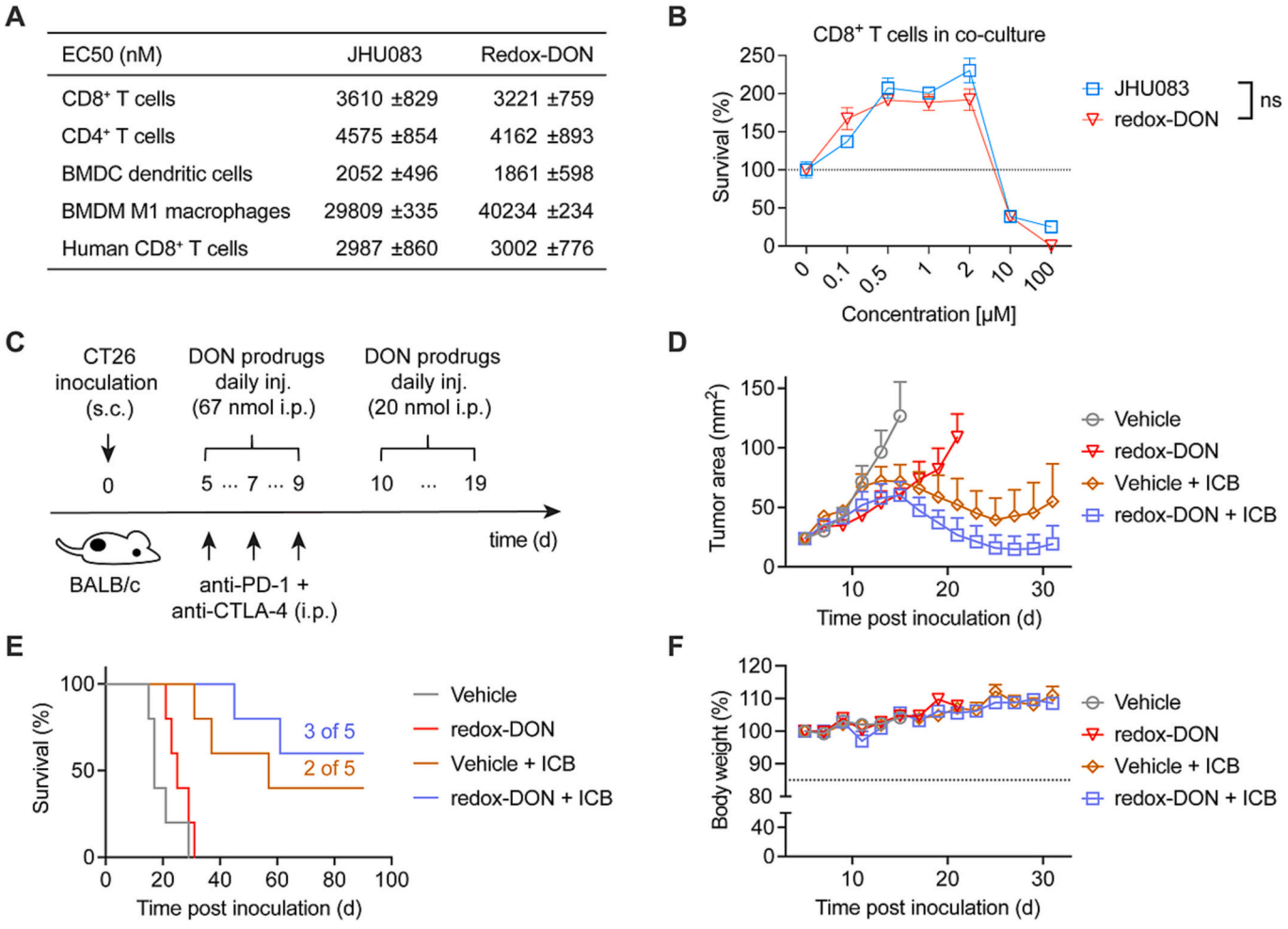

Fig. 5. Redox-DON is well tolerated by immune cells and synergizes with checkpoint inhibitors. (A) EC_{50} values (mean ± s.e.m) derived from dose-response curves of DON prodrug-treated immune cells. (B) Dose-response curves of P_{mel} $CD8^+$ T cells in co-culture with B16F10 cells in an effector-to-target (E:T) ratio of 1:5. The error bars present the data as mean ± s.e.m. All experiments were performed at least twice. (C—F) BALB/c mice were inoculated subcutaneously with CT26 tumor cells (0.3×10^6) and received from day 5 on i.p. 3 doses of checkpoint inhibitors anti-PD-1 (200 μg/injection) and anti-CTLA-4 (100 μg/injection) plus vehicle or redox-DON daily until day 19 according to the reported dosing schedule of JHU083 ($n = 5$ mice). Mice were euthanized when the tumor size of individual mice reached 150 mm^2. Shown are the schematic illustration of treatment schedule (C), average tumor growth curves (D), survival curves (E), and average body weight curves (F).

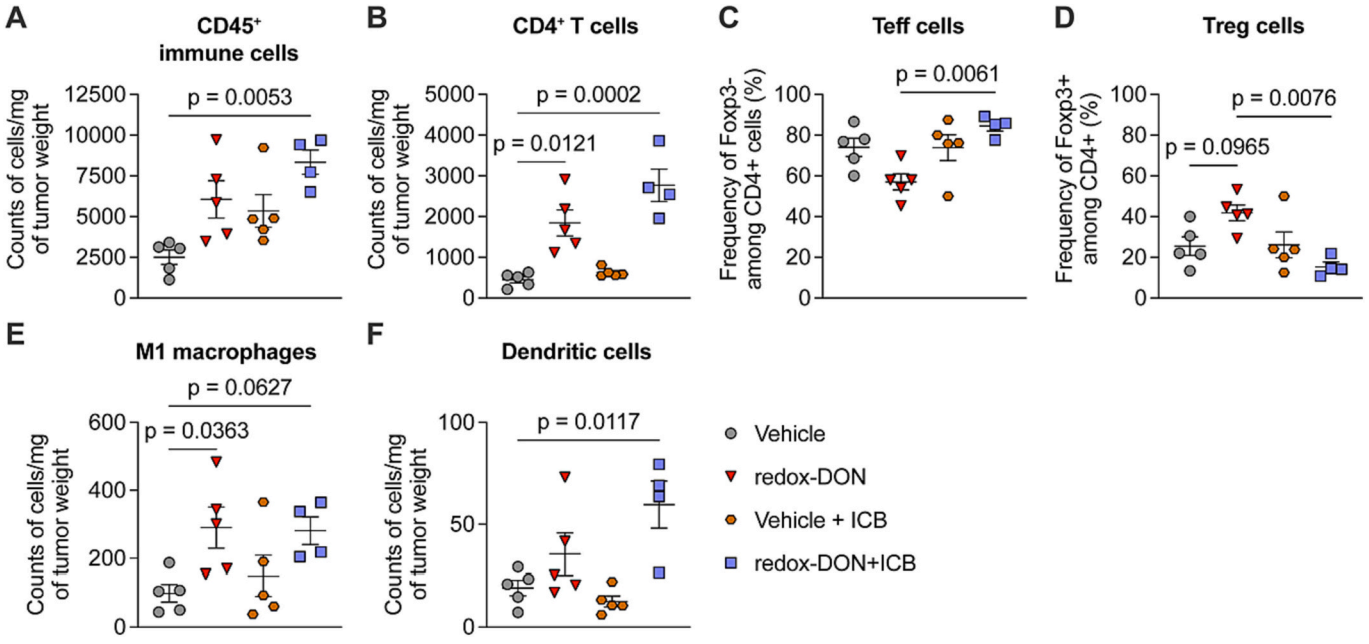

Fig. 6. Redox-DON increases immune cells infiltration in the tumor. BALB/c mice were inoculated subcutaneously with CT26 tumor cells (0.3×10^6) and received from day 9 on 3 doses of checkpoint inhibitors including anti-PD-1 (200 μg, i.p.) and anti-CTLA-4 (100 μg, i.p.) plus daily injection (i.p.) of vehicle or redox-DON at a dose of 67 nmol for 5 days, followed by a dose of 20 nmol for 4 days. Mice were euthanized on day 16 and the tumors were processed for flow cytometry analyses ($n = 5$ mice). Shown are $CD45^+$ tumor infiltrating leucocytes (A), $CD4^+$ TILs (B), Teff cells (C), Treg cells (D), M1 macrophages (E), and dendritic cells (F).

(Fig. 6C), but not the regulatory T cells (Treg, defined as $Foxp3^+CD4^+$), as the frequency of Treg cells was decreased in the combination group as compared to the redox-DON-treated group (Fig. 6D). Moreover, we noticed that the treatment with redox-DON led to the increase of antigen-presenting cells in tumor including M1 macrophages (defined as $CD45^+CD8^-CD4^-CD11b^+Gr\text{-}1^-MHCII^+$) and dendritic cells (defined as $CD45^+CD8^-CD4^-CD11c^+Gr\text{-}1^-MHCII^+$) in mice treated with the combination of ICB + redox-DON (Fig. 6E-F).

The $CD45^+$ lymphocyte counts in the tumor-draining lymph node were increased in the ICB-treated groups, but not in the vehicle or redox-DON only groups (Fig. S8A). Increased CD45+, CD4+ and CD8+ cell counts were more prominent in the redox-DON+ICB group in comparison to the ICB only group (Fig. S8B—C). No significant changes were observed for the counts of immune cells in the peripheral blood (Fig. S8D-E).

4. Discussion

Among several metabolic hallmarks of cancer, the increased demand of glutamine is a particular metabolic vulnerability that can be explored in anti-cancer therapy. We synthesized and characterized a novel glutamine inhibitor, redox-DON, which was selectively activated in response to elevated reducing activity in the TME and showed promise as a safe and effective therapeutic drug for tumor-targeted glutamine inhibition. The approach of reversible chemical modification can be potentially generalized for mitigating high toxicity of promising drugs.

Glutamine inhibition by DON prodrugs can abrogate the complete glutamine metabolism in cells. However, the safety of applying such inhibitor as a therapeutic drug has to be addressed. While the previously reported DON prodrugs all relied on protease-responsive pro-moieties [20,33], we chose a redox-responsive design to target the TME. The redox-DON prodrug increased the safety towards the GI tract and spleen tissue in comparison to the state-of-the-art DON prodrug JHU083, while maintaining equivalent efficacy. In a dose escalation study, we found an approximate threefold decrease of toxicity as manifested in similar side effects caused by the low dose JHU083 (67 nmol) treatment as compared to the high dose redox-DON (200 nmol) treatment. The histology results indicate a reduction of EMH in the spleen of JHU083 (200 nmol)-treated mice compared to control and redox-DON-treated animals which may reflect an augmented need of immune cells in the ulcerated colon. Usually, mild to moderate EMH in the spleen is a normal finding in young mice, as the need of new blood and immune cells is higher in juvenile compared to adult mice [34].

During the preparation of this paper, a study appeared in which the protease-responsive prodrug JHU083 was further developed to DRP-104 [33]. This new prodrug comprises a more sophisticated protease-responsive design, which focused on the reduction of the toxicity to the GI tract. DRP-104 was found after an extensive screen and from the comparison with JHU083 seemed to show similar safety profile as the redox-DON reported here [33]. Our results suggest that chemical-based prodrug design, such as the redox-responsive strategy, is also promising in addition to the protease-responsive delivery system for tumor-targeted metabolic modulation.

Similar as JHU083, treatment with redox-DON increased immune cell infiltration in the tumor, in particular $CD4^+$ T cells, M1 macrophages, and dendritic cells. The effect of glutamine inhibition together with checkpoint blockade in the CT26 mouse colon cancer model shows the potential of combining metabolic reprogramming of the TME with existing immunotherapies. Together with previous findings, the results suggest that DON prodrugs mainly affect cancer cells rather than immune cells in the TME. Immune cells can increase their glucose uptake and better survive in the glutamine-inhibited environment [12,13]. Tumor cell death in response to DON prodrug treatment and the subsequent secretion of danger-associated signals may promote recruitment of anti-tumor associated macrophages as well as other immune cells such as dendritic cells and T cells [11,13], which further enhance antigen presentation and the cytotoxic response in the tumor. Several previous reports showed that M2 macrophages could be skewed to an M1 phenotype in a glutamine-deprived microenvironment [14]. In addition, we found treatment with redox-DON increased M1 macrophages in the TME, thereby supporting previous observations. This phenotype is pronounced when not only glutamine to glutamate conversion by GLS1, but also glutamine synthetase (GLUL) is inhibited [35].

As suggested in previous reports with JHU083, the combination of

glutamine inhibitors with ICB can increase the therapeutic efficacy in comparison to the single agent treatments [12,13]. Here, we used the combination of anti-PD1 and anti-CTLA-4 as the ICB therapy, which skewed CD4+ TILs from Treg to Teff phenotypes. This effect has been mostly attributed to the treatment with anti-CTLA-4, while anti-PD1 prevents T cell exhaustion in the tumor [36].

5. Conclusion

Our results suggest that the novel redox-responsive DON prodrug could improve the safety of glutamine inhibition therapy in comparison to the protease-responsive JHU083, while maintaining equivalent efficacy. The combination of redox-DON with checkpoint inhibitors improved the efficacy of ICB treatment, which indicates a potential role of glutamine inhibition in combination with ICB therapy for patients in which ICB alone cannot lead to the expected outcomes. This report suggests an important role of antigen-presenting cells and $CD4^+$ T cells for the synergy of DON prodrugs and ICB. Overall, the detailed mechanisms of glutamine inhibition through DON prodrugs will need further investigation.

Credit author statement

C.P., N.B., L.T. and X.H. designed the experiments and interpreted the results. C.P. synthesized and characterized the chemical compounds. N.B. performed the release studies with redox-DON. D.O. contributed with technical advice in mass spectrometry. C.P. and N.B. carried out the animal experiments and *in vitro* studies. C.P., B.F. and N.B. performed animal sacrifices and processed tissues for analysis. C.P. carried out the flow cytometry analysis and analyzed the results. C.P. and N.B. prepared the histology samples. C.G. and C.P. interpreted the histology results. C.P., N.B. L.T. and X.H. wrote the manuscript with input from other authors.

CRediT authorship contribution statement

Céline Jasmin Prange: Writing – review & editing, Writing – original draft, Methodology, Formal analysis, Data curation, Conceptualization. **Nadia Yasmina Ben Sayed:** Writing – review & editing, Methodology, Formal analysis, Data curation. **Bing Feng:** Methodology, Formal analysis. **Christine Goepfert:** Methodology, Formal analysis. **Daniel Ortiz Trujillo:** Methodology. **Xile Hu:** Writing – review & editing, Supervision, Funding acquisition, Conceptualization. **Li Tang:** Writing – review & editing, Writing – original draft, Supervision, Funding acquisition, Formal analysis, Conceptualization.

Declaration of competing interest

C.P., N.B., L.T. and X.H. are inventors on a filed patent related to the redox-DON. L.T. is a co-founder, share-holder, and advisor for Leman Biotech. The interests of L.T. were reviewed and managed by EPFL. The remaining authors declare no competing interests.

Data availability

All data associated with this study are present in the paper or the Supplementary Materials. All raw data is available upon request.

Acknowledgements

The authors thank the teams of the Flow Cytometry Core Facility, the Histology Core Facility and the NMR service at EPFL for their advice. This work was supported by EPFL and the Swiss National Science Foundation (200021_181977). L.T. acknowledges the grant support from Swiss National Science Foundation (315230_204202, IZLCZ0_206035, CRSII5_205930), European Research Council under the ERC grant agreement MechanoIMM (805337), Swiss Cancer Research Foundation (KFS-4600-08-2018), Kristian Gerhard Jebsen Foundation, Anna Fuller Fund, Xtalpi Inc., and EPFL.

Appendix A. Supplementary data

Supplementary data to this article can be found online at https://doi.org/10.1016/j.jconrel.2024.02.031.

References

[1] C.-H. Chang, J. Qiu, D. O'Sullivan, M.D. Buck, T. Noguchi, J.D. Curtis, Q. Chen, M. Gindin, M.M. Gubin, G.J.W. van der Windt, E. Tonc, R.D. Schreiber, E.J. Pearce, E.L. Pearce, Metabolic competition in the tumor microenvironment is a driver of Cancer progression, Cell. 162 (2015) 1229–1241, https://doi.org/10.1016/j.cell.2015.08.016.
[2] N. Kedia-Mehta, D.K. Finlay, Competition for nutrients and its role in controlling immune responses, Nat. Commun. 10 (2019) 2123, https://doi.org/10.1038/s41467-019-10015-4.
[3] Z.E. Stine, Z.T. Schug, J.M. Salvino, C.V. Dang, Targeting cancer metabolism in the era of precision oncology, Nat. Rev. Drug Discov. 21 (2022) 141–162, https://doi.org/10.1038/s41573-021-00339-6.
[4] K.M. Lemberg, S.S. Gori, T. Tsukamoto, R. Rais, B.S. Slusher, Clinical development of metabolic inhibitors for oncology, J. Clin. Investig. 132 (2022) e148550, https://doi.org/10.1172/JCI148550.
[5] L. Hagenfeldt, A. Arvidsson, The distribution of amino acids between plasma and erythrocytes, Clin. Chim. Acta 100 (1980) 133–141, https://doi.org/10.1016/0009-8981(80)90074-1.
[6] J. Jiang, S. Srivastava, J. Zhang, Starve Cancer cells of glutamine: break the spell or make a hungry monster? Cancers. 11 (2019) 804, https://doi.org/10.3390/cancers11060804.
[7] Z. Wang, F. Liu, N. Fan, C. Zhou, D. Li, T. Macvicar, Q. Dong, C.J. Bruns, Y. Zhao, Targeting Glutaminolysis: new perspectives to understand Cancer development and novel strategies for potential target therapies, Front. Oncol. 10 (2020) 589508, https://doi.org/10.3389/fonc.2020.589508.
[8] H.C. Yoo, Y.C. Yu, Y. Sung, J.M. Han, Glutamine reliance in cell metabolism, Exp. Mol. Med. 52 (2020) 1496–1516, https://doi.org/10.1038/s12276-020-00504-8.
[9] Y. Zhao, X. Zhao, V. Chen, Y. Feng, L. Wang, C. Croniger, R.A. Conlon, S. Markowitz, E. Fearon, M. Puchowicz, H. Brunengraber, Y. Hao, Z. Wang, Colorectal cancers utilize glutamine as an anaplerotic substrate of the TCA cycle in vivo, Sci. Rep. 9 (2019) 19180, https://doi.org/10.1038/s41598-019-55718-2.
[10] Y. Niu, T. Mayr, M.H. Muders, Competition for nutrients or cell intrinsic programming? – metabolic mechanisms behind the tumor promoting immune microenvironment in cancer, Sig Transduct Target Ther. 6 (2021) 279, https://doi.org/10.1038/s41392-021-00693-2.
[11] J. Jin, J.-K. Byun, Y.-K. Choi, K.-G. Park, Targeting glutamine metabolism as a therapeutic strategy for cancer, Exp. Mol. Med. 55 (2023) 706–715, https://doi.org/10.1038/s12276-023-00971-9.
[12] R.D. Leone, L. Zhao, J.M. Englert, I.-M. Sun, M.-H. Oh, I.-H. Sun, M.L. Arwood, I. A. Bettencourt, C.H. Patel, J. Wen, A. Tam, R.L. Blosser, E. Prchalova, J. Alt, R. Rais, B.S. Slusher, J.D. Powell, Glutamine blockade induces divergent metabolic programs to overcome tumor immune evasion, Science. 366 (2019) 1013–1021, https://doi.org/10.1126/science.aav2588.
[13] M.-H. Oh, I.-H. Sun, L. Zhao, R.D. Leone, I.-M. Sun, W. Xu, S.L. Collins, A.J. Tam, R. L. Blosser, C.H. Patel, J.M. Englert, M.L. Arwood, J. Wen, Y. Chan-Li, L. Tenora, P. Majer, R. Rais, B.S. Slusher, M.R. Horton, J.D. Powell, Targeting glutamine metabolism enhances tumor-specific immunity by modulating suppressive myeloid cells, J. Clin. Investig. 130 (2020) 3865–3884, https://doi.org/10.1172/JCI131859.
[14] E.M. Palmieri, A. Menga, R. Martín-Pérez, A. Quinto, C. Riera-Domingo, G. De Tullio, D.C. Hooper, W.H. Lamers, B. Ghesquière, D.W. McVicar, A. Guarini, M. Mazzone, A. Castegna, Pharmacologic or genetic targeting of glutamine Synthetase skews macrophages toward an M1-like phenotype and inhibits tumor metastasis, Cell Rep. 20 (2017) 1654–1666, https://doi.org/10.1016/j.celrep.2017.07.054.
[15] M.I. Gross, S.D. Demo, J.B. Dennison, L. Chen, T. Chernov-Rogan, B. Goyal, J. R. Janes, G.J. Laidig, E.R. Lewis, J. Li, A.L. MacKinnon, F. Parlati, M.L. M. Rodriguez, P.J. Shwonek, E.B. Sjogren, T.F. Stanton, T. Wang, J. Yang, F. Zhao, M.K. Bennett, Antitumor activity of the Glutaminase inhibitor CB-839 in triple-negative breast Cancer, Mol. Cancer Ther. 13 (2014) 890–901, https://doi.org/10.1158/1535-7163.MCT-13-0870.
[16] H. Jin, S. Wang, E.A. Zaal, C. Wang, H. Wu, A. Bosma, F. Jochems, N. Isima, G. Jin, C. Lieftink, R. Beijersbergen, C.R. Berkers, W. Qin, R. Bernards, A powerful drug combination strategy targeting glutamine addiction for the treatment of human liver cancer, eLife 9 (2020), https://doi.org/10.7554/eLife.56749.
[17] M.T. Grinde, B. Hilmarsdottir, H.M. Tunset, I.M. Henriksen, J. Kim, M.H. Haugen, M.B. Rye, G.M. Mælandsmo, S.A. Moestue, Glutamine to proline conversion is associated with response to glutaminase inhibition in breast cancer, Breast Cancer Res. 21 (2019) 61, https://doi.org/10.1186/s13058-019-1141-0.
[18] A.A. Cluntun, M.J. Lukey, R.A. Cerione, J.W. Locasale, Glutamine metabolism in Cancer: understanding the heterogeneity, Trends in Cancer. 3 (2017) 169–180, https://doi.org/10.1016/j.trecan.2017.01.005.

[19] K.M. Lemberg, J.J. Vornov, R. Rais, B.S. Slusher, We're not "DON" yet: optimal dosing and prodrug delivery of *6-Diazo-5-oxo-L-norleucine*, Mol. Cancer Ther. 17 (2018) 1824–1832, https://doi.org/10.1158/1535-7163.MCT-17-1148.
[20] R. Rais, A. Jančařík, L. Tenora, M. Nedelcovych, J. Alt, J. Englert, C. Rojas, A. Le, A. Elgogary, J. Tan, L. Monincová, K. Pate, R. Adams, D. Ferraris, J. Powell, P. Majer, B.S. Slusher, Discovery of 6-Diazo-5-oxo- L -norleucine (DON) prodrugs with enhanced CSF delivery in monkeys: a potential treatment for glioblastoma, J. Med. Chem. 59 (2016) 8621–8633, https://doi.org/10.1021/acs.jmedchem.6b01069.
[21] T.M. Antalis, T. Shea-Donohue, S.N. Vogel, C. Sears, A. Fasano, Mechanisms of disease: protease functions in intestinal mucosal pathobiology, Nat. Rev. Gastroenterol. Hepatol. 4 (2007) 393–402, https://doi.org/10.1038/ncpgasthep0846.
[22] C. López-Otín, J.S. Bond, Proteases: multifunctional enzymes in life and disease, J. Biol. Chem. 283 (2008) 30433–30437, https://doi.org/10.1074/jbc.R800035200.
[23] L. Kennedy, J.K. Sandhu, M.-E. Harper, M. Cuperlovic-Culf, Role of glutathione in Cancer: from mechanisms to therapies, Biomolecules. 10 (2020) 1429, https://doi.org/10.3390/biom10101429.
[24] E.H. Cheteh, M. Augsten, H. Rundqvist, J. Bianchi, V. Sarne, L. Egevad, V.J. Bykov, A. Östman, K.G. Wiman, Human cancer-associated fibroblasts enhance glutathione levels and antagonize drug-induced prostate cancer cell death, Cell Death Dis. 8 (2017) e2848, https://doi.org/10.1038/cddis.2017.225.
[25] L. Tang, Y. Zheng, M.B. Melo, L. Mabardi, A.P. Castaño, Y.-Q. Xie, N. Li, S. B. Kudchodkar, H.C. Wong, E.K. Jeng, M.V. Maus, D.J. Irvine, Enhancing T cell therapy through TCR-signaling-responsive nanoparticle drug delivery, Nat. Biotechnol. (2018), https://doi.org/10.1038/nbt.4181.
[26] L. Wei, Y. Zhao, X. Hu, L. Tang, Redox-responsive Polycondensate Neoepitope for enhanced personalized Cancer vaccine, ACS Cent. Sci. 6 (2020) 404–412, https://doi.org/10.1021/acscentsci.9b01174.
[27] Y. Zhao, Y.-Q. Xie, S. Van Herck, S. Nassiri, M. Gao, Y. Guo, L. Tang, Switchable immune modulator for tumor-specific activation of anticancer immunity, Sci. Adv. 7 (2021) eabg7291, https://doi.org/10.1126/sciadv.abg7291.
[28] A. Rahman, P. Frederick, P. Smith, Van T. Luc, Paul V. Woolley, Phase I study and clinical pharmacology of 6-diazo-5-oxo-L-norleucine (DON), Investig. New Drugs 3 (1985), https://doi.org/10.1007/BF00170760.
[29] J. Alt, M.C. Potter, C. Rojas, B.S. Slusher, Bioanalysis of 6-diazo-5-oxo-l-norleucine in plasma and brain by ultra-performance liquid chromatography mass spectrometry, Anal. Biochem. 474 (2015) 28–34, https://doi.org/10.1016/j.ab.2015.01.001.
[30] D.R. Wise, C.B. Thompson, Glutamine addiction: a new therapeutic target in cancer, Trends Biochem. Sci. 35 (2010) 427–433, https://doi.org/10.1016/j.tibs.2010.05.003.
[31] B.-R. Jin, K.-S. Chung, S.-Y. Cheon, M. Lee, S. Hwang, S. Noh Hwang, K.-J. Rhee, H.-J. An, Rosmarinic acid suppresses colonic inflammation in dextran sulphate sodium (DSS)-induced mice via dual inhibition of NF-κB and STAT3 activation, Sci. Rep. 7 (2017) 46252, https://doi.org/10.1038/srep46252.
[32] L. Dong, J. Xie, Y. Wang, H. Jiang, K. Chen, D. Li, J. Wang, Y. Liu, J. He, J. Zhou, L. Zhang, X. Lu, X. Zou, X.-Y. Wang, Q. Wang, Z. Chen, D. Zuo, Mannose ameliorates experimental colitis by protecting intestinal barrier integrity, Nat. Commun. 13 (2022) 4804, https://doi.org/10.1038/s41467-022-32505-8.
[33] R. Rais, K.M. Lemberg, L. Tenora, M.L. Arwood, A. Pal, J. Alt, Y. Wu, J. Lam, J.M. H. Aguilar, L. Zhao, D.E. Peters, C. Tallon, R. Pandey, A.G. Thomas, R.P. Dash, T. Seiwert, P. Majer, R.D. Leone, J.D. Powell, B.S. Slusher, Discovery of DRP-104, a tumor-targeted metabolic inhibitor prodrug, Sci. Adv. 8 (2022) eabq5925, https://doi.org/10.1126/sciadv.abq5925.
[34] C.L. Willard-Mack, S.A. Elmore, W.C. Hall, J. Harleman, C.F. Kuper, P. Losco, J. E. Rehg, C. Rühl-Fehlert, J.M. Ward, D. Weinstock, A. Bradley, S. Hosokawa, G. Pearse, B.W. Mahler, R.A. Herbert, C.M. Keenan, Nonproliferative and proliferative lesions of the rat and mouse Hematolymphoid system, Toxicol. Pathol. 47 (2019) 665–783, https://doi.org/10.1177/0192623319867053.
[35] N.N. Pavlova, S. Hui, J.M. Ghergurovich, J. Fan, A.M. Intlekofer, R.M. White, J. D. Rabinowitz, C.B. Thompson, J. Zhang, As Extracellular Glutamine Levels Decline, Asparagine Becomes an Essential Amino Acid, Cell Metab. 27 (2018) 428–438.e5, https://doi.org/10.1016/j.cmet.2017.12.006.
[36] A.D. Waldman, J.M. Fritz, M.J. Lenardo, A guide to cancer immunotherapy: from T cell basic science to clinical practice, Nat. Rev. Immunol. 20 (2020) 651–668, https://doi.org/10.1038/s41577-020-0306-5.